GAIN MODULATION OF CHOLINERGIC NEURONS IN THE MEDIAL SEPTUM-DIAGONAL BAND OF BROCA AND THE MECHANISM OF CHOLINERGIC SUPPRESSION OF HIPPOCAMPAL RIPPLES

by

Eric D. Melonakos

A dissertation submitted to the faculty of
The University of Utah
in partial fulfillment of the requirements for the degree of

Doctor of Philosophy

Department of Bioengineering

The University of Utah

August 2017

The University of Utah Graduate School

STATEMENT OF DISSERTATION APPROVAL

The dissertation of **Eric D. Melonakos**

has been approved by the following supervisory committee members:

Fernando R. Fernandez	, Chair	**5/12/2017** Date Approved
John A. White	, Member	**5/12/2017** Date Approved
Alan D. Dorval	, Member	**5/12/2017** Date Approved
Richard D. Rabbitt	, Member	**5/12/2017** Date Approved
Alla R. Borisyuk	, Member	**5/12/2017** Date Approved

and by **David W. Grainger** , Chair/Dean of

the Department/College/School of **Bioengineering**

and by David B. Kieda, Dean of The Graduate School.

ABSTRACT

Hippocampal network oscillations are important for learning and memory. Theta rhythms are involved in attention, navigation, and memory encoding, whereas sharp wave-ripple complexes (ripples) are involved in memory consolidation. Cholinergic neurons in the medial septum-diagonal band of Broca (MS-DB) influence both types of hippocampal oscillations, promoting theta rhythms and suppressing ripples. They also receive frequency-dependent hyperpolarizing feedback from hippocamposeptal connections, potentially affecting their role as neuromodulators in the septohippocampal circuit. However, little is known about how the integration properties of cholinergic MS-DB neurons change with hyperpolarization. By potentially altering firing behavior in cholinergic neurons, hyperpolarizing feedback from the hippocampal neurons may, in turn, change hippocampal network activity. To study how hyperpolarizing inputs change in membrane integration properties, we used whole-cell patch-clamp recordings targeting genetically labeled, choline acetyltransferase-positive neurons in mouse medial septal brain slices. Hyperpolarization of cholinergic MS-DB neurons resulted in a long-lasting decrease in spike firing rate and input-output gain. Additionally, voltage-clamp measures implicated a slowly inactivating, 4-AP-insensitive, outward K^+ conductance. Using a conductance-based model of cholinergic MS-DB neurons, we show that the ability of this conductance to modulate firing rate and gain depends on the expression of an experimentally verified shallow intrinsic spike frequency-voltage relationship. Finally,

we show that cholinergic suppression of hippocampal ripples can be achieved through an imbalance in drive, caused by cholinergic modulation, to hippocampal excitatory and inhibitory neurons. Together, these findings show possible mechanisms through which cholinergic MS-DB neurons may both influence and be influenced by hippocampal rhythms.

To my family, who taught me a love of learning for learning's sake.

TABLE OF CONTENTS

ABSTRACT iii

LIST OF FIGURES viii

ACKNOWLEDGEMENTS x

Chapters

1. INTRODUCTION 1

1.1 Learning and memory in the hippocampus 1
1.2 Electrical oscillations in the hippocampus 2
1.3 The medial septum-diagonal band of Broca regulates theta and sharp wave-ripples 4
1.4 Physiology of cholinergic neurons in the MS-DB 6
1.5 Cholinergic MS-DB neurons influence hippocampal theta 7
1.6 Cholinergic MS-DB neurons influence hippocampal sharp wave-ripples 9
1.7 Gain changes in cholinergic MS-DB neurons and the mechanism of cholinergic modulation of hippocampal ripples 10

2. GAIN MODULATION OF CHOLINERGIC NEURONS IN THE MEDIAL SEPTUM-DIAGONAL BAND OF BROCA THROUGH HYPERPOLARIZATION ... 11

2.1 Abstract 12
2.2 Introduction 12
2.3 Materials and methods 13
2.3.1 Tissue preparation 13
2.3.2 Electrophysiology 13
2.3.3 Simulations 13
2.3.4 Data analysis 14
2.4 Results 15
2.4.1 Hyperpolarization reduces firing rate and gain in cholinergic MS-DB neurons 15
2.4.2 Voltage dependence, time dependence, and recovery time of hyperpolarization-induced firing rate reduction 15
2.4.3 4-AP-sensitive currents are not responsible for hyperpolarization-mediated changes in input-output properties 17
2.4.4 Cholinergic MS-DB neurons express a slowly activating and inactivating, voltage-gated K^+ current 18

2.4.5 Reduced firing rate and gain is associated with minimal changes in spike shape 19
2.4.6 The introduction of a slowly inactivating, outward K^+ current allows for a subtractive, but not divisive, change in the *f-I* curve of a model neuron with a steep *f-V* curve 22
2.4.7 Cholinergic MS-DB neurons have shallow *f-V* curves 22
2.4.8 Gain changes through the introduction of a slowly inactivating K^+ current require shallow *f-V* curves in an eLIF model 23
2.5 Discussion 24
2.5.1 Implications for cholinergic MS-DB neuron control of hippocampal theta oscillations 24
2.5.2 Implications for cholinergic MS-DB neuron control of hippocampal SPW-Rs 25
2.5.3 Voltage-dependent gain modulation in cholinergic MS-DB neurons 26
2.5.4 Identity of the slowly inactivating outward current 26
2.6 References 27

3. CHOLINERGIC SUPPRESSION OF HIPPOCAMPAL RIPPLES THROUGH DISRUPTION OF BALANCED EXCITATION/INHIBITION 29

3.1 Abstract 29
3.2 Introduction 30
3.3 Materials and methods 31
3.3.1 Model architecture 31
3.3.2 Data analysis 34
3.4 Results 35
3.4.1 Balancing the effects of I_{DC} on steady-state voltage preserves ripples 36
3.4.2 I_{DC} drives the network towards one of two types of subnetworks 40
3.4.3 Shifts in network frequency can be reversed through preferential input to each neuron type 43
3.5 Discussion 49
3.5.1 Implications for hippocampal ripple modulation by ACh 49
3.5.2 Accuracy of the simplified model of cholinergic suppression of ripples 50

4. DISCUSSION 53

4.1 Summary of results 53
4.1.1 Cholinergic neuron response to hyperpolarizing inputs 53
4.1.2 Mechanism of cholinergic suppression of hippocampal ripples 55
4.2 Effects of gain changes in cholinergic MS-DB neurons on neural rhythms 56
4.3 The role of balanced excitation and inhibition in hippocampal rhythms 60

REFERENCES 62

LIST OF FIGURES

Figures

2.1 Hyperpolarization of cholinergic MS-DB neurons caused a reduction in firing rate....16

2.2 Hyperpolarization of cholinergic MS-DB neurons caused a divisive effect on the *f-I* curve....17

2.3 Characterization of the voltage dependence, time dependence, and recovery time of the hyperpolarization-induced firing rate reduction....18

2.4 4-AP-sensitive currents were not responsible for the divisive change in the *f-I* curve....19

2.5 Voltage-clamp measures revealed the presence of a slow inactivating, outward current....20

2.6 Characterization of spike shape following hyperpolarization....21

2.7 eLIF model (Δ_T = 2 mV) with a slowly inactivating K^+ current (I_{siK}) and steep *f-V* curve shows a subtractive change in the *f-I* curve....23

2.8 Cholinergic neurons in the MS-DB had shallow *f-V* curves....24

2.9 eLIF model (Δ_T = 10 mV) with I_{siK} and a shallow *f-V* curve shows a divisive change in the *f-I* curve....25

3.1 Model of ripples from Brunel and Wang (2003) replicates hippocampal features...32

3.2 The balance of I_{DC}, a surrogate for cholinergic input from the MS-DB, in both types of neurons determines the resulting effects on ripple ratio and frequency....39

3.3 Increases in I_{DCpyr} emphasize the E-I-E network, while increases in I_{DCint} emphasize the I-I network....42

3.4 The frequency of a network with a slower GABAergic time constant can be raised with increased drive to the I-I subnetwork....45

3.5 In networks with varied intrinsic frequencies, preferential input to each neuron type can adjust overall network frequency 47

ACKNOWLEDGEMENTS

The successful completion of this work is the result of the efforts of many people over the past seven years. I could not have completed this PhD without their help, and I owe all of them thanks for their various contributions.

Specifically, Fernando Fernandez has been an exceptional advisor spending countless hours in the lab and over the phone listening to and instructing me. He taught me with patience, even when I asked the same questions over and over again. He deserves thanks not only for guiding me in my experiments and analyses but also for contributing the original idea and associated model for Chapter 2. The steep learning curve of electrophysiological research would have been insurmountable without his help.

John White also deserves my gratitude and recognition for his role as my official advisor for the majority of my PhD. He guided my projects, provided helpful feedback in lab meetings and one-on-one meetings, and contributed the financial support I needed to complete my PhD. As with Fernando, John's patience was key in my development as a scientist, and I owe him my thanks.

Alan "Chuck" Dorval has willingly served as a "foster" advisor to me during the past couple years, following John and Fernando's move to Boston University. He offered space in his lab, health insurance money, and even a project idea. Even when that project did not pan out, he continued to sacrifice time in advising me in a project completely unrelated to his lab's research. And I would be remiss if I did not mention the great fun

we had playing disc golf and bowling!

My other committee and lab members have also provided selfless help and been great friends. Mike Economo, Tilman Broicher, Joey Martinez, Paola Malerba, Nathan Smith, Katherine Lambert, Felix Furmanov, Heidi Febinger, Marsa Taheri, Collin Anderson, Mike Gee, and Christian Polar have each helped in their own way. All have been kind.

Finally, my family deserves my infinite gratitude for their examples, encouragement, and love. From the time I learned as a child about my grandfather's PhD, I've wanted to reach this pinnacle of education. With my parents' encouragement and my oldest brothers' advice, I made it to where I am. My other siblings and family members have likewise been crucial in my successes throughout my education. Most recently, my wife, Quincey McGuire, has provided the most constant and intense support to me. I couldn't have done it without her. Through countless conversations, worries, prayers, failures, and successes, these have all been by my side. Thank you!

CHAPTER 1

INTRODUCTION

1.1 Learning and memory in the hippocampus

The hippocampus is a brain structure in the limbic system, located in the medial temporal lobe. During the past century, the hippocampus has been the subject of a great deal of research. In recent decades, perhaps most notably beginning with observations of patient Henry Molaison (Scoville and Milner, 1957), research has largely focused on the role of the hippocampus in learning and memory. The hippocampus has roles in the encoding and consolidation of declarative memories (Squire, 1992; Buzsáki, 2015). Much of the literature about the hippocampus has focused on rodents, where the hippocampus is also crucial for learning and memory, including cue relationships (Sutherland et al., 1989), water mazes (Sutherland and McDonald, 1990), and spatial memory (O'Keefe and Nadel, 1978; Morris et al., 1982; Aggleton et al., 1986).

Spatial memory, in particular, has received much attention, possibly because of the various cell types within the limbic system that are involved in navigation. Within the hippocampus, place cells have been identified that reliably fire when the animal is at specific locations within an environment (O'Keefe, 1976; O'Keefe et al., 1998). Head direction cells have also been identified, which reside in the postsubiculum and encode information about the direction an animal's head is pointing (Taube et al., 1990; Taube,

2007). Adding to its involvement in spatial memory, the hippocampus receives input from other regions of the brain involved in navigation, including the medial entorhinal cortex (Steward and Scoville, 1976; Witter and Amaral, 1991; Bush et al., 2014). Within the medial entorhinal cortex, grid cells fire at spatially periodic locations in an environment (Hafting et al., 2005), and boundary cells fire at locations close to environmental boundaries (Solstad et al., 2008). Each of these cell types makes up part of the processing of rich spatial information in the limbic system and, specifically, the hippocampus.

1.2 Electrical oscillations in the hippocampus

Perhaps the most prominent physiological correlate of learning and memory in the hippocampus is the local field potential (LFP). Stereotyped patterns of LFP electrical oscillations have been observed in rodents. Among these are hippocampal theta rhythms and sharp wave-ripple complexes (ripples). Although both of these rhythms are thought to be critical for information processing, including memory and navigation, they occur during opposing behaviors. Specifically, theta rhythms (4-12 Hz) occur during exploration and REM sleep and are correlated with a variety of behaviors, such as attention, navigation, and memory encoding (Berry and Thompson, 1978; Winson, 1978; see Buzsáki, 2005, for review; Hasselmo, 2005). On the other hand, ripples (140-220 Hz; O'Keefe, 1976) occur during immobility and slow wave sleep (Buzsáki et al., 1983, 1992) and are involved in memory consolidation (Girardeau et al., 2009; Maingret et al., 2016).

During *in vivo* theta, hippocampal pyramidal neurons have slow overall firing

rates (~5 spikes/s, and almost always under 10 spikes/s; Ranck, 1973; Hirase et al., 1999) and elicit bursts of spiking activity at theta frequencies (Harvey et al., 2009), while interneurons firing rates peak anywhere from 29-147 spikes/s (Ranck, 1973). Place cells (pyramidal cells) have slow firing rates (0.6-4.7 Hz), which depend on the animal's location relative to its place field (Harvey et al., 2009). The theta phase of place cell firing also depends on the animal's position in the place field; as the animal moves through the place field the phase of spiking relative to the theta oscillation advances (O'Keefe and Recce, 1993; Skaggs et al., 1996). Average pyramidal neurons' firing occurs at the peak of the theta oscillation (when measured at the outer molecular layer of the dentate) (Fox et al., 1986), whereas the firing of interneurons precedes pyramidal neurons by 20 to 60 degrees, depending on the interneuron type (Skaggs et al., 1996; Csicsvari et al., 1999).

In contrast, ripples are initiated with increased external drive from CA3 (Chrobak and Buzsáki, 1996; Csicsvari et al., 2000; Bezaire and Soltesz, 2013). Ripple events typically last about 50 ms and arrive at a frequency of about 1-2 Hz (Malerba et al., 2016). These rhythms are characterized by balanced excitation and inhibition in pyramidal neurons *in vivo* (English et al., 2014). Although balanced, inhibition lags behind excitation (Maier et al., 2011; Hulse et al., 2016). Individual neurons fire at low rates (relative to the LFP ripple frequency) and exhibit irregular firing patterns that are independent of synchronous population rates (Fries et al., 2001; Logothetis et al., 2001). During ripples *in vivo*, the average firing rate of projection interneurons is ~50 Hz (Jinno et al., 2007).

The specific sequence of place cell spikes during an experience is called a "neural

ensemble". During ripple oscillations, neural ensembles from near future or recent past experience are played. The playing of neural ensembles representing future experience is called preplay (Dragoi and Tonegawa, 2012). Preplay events are thought to select from a repertoire of cell assemblies that will encode future novel experiences (Dragoi and Tonegawa, 2013, 2014). The playing of neural ensembles representing previous experience is called replay (Wilson and McNaughton, 1994; Davidson et al., 2009) and is compressed in time (Nádasdy et al., 1999; Ji and Wilson, 2007). Replay events are thought to be important for consolidating experiences to long-term storage in the cortex (Wei et al., 2016). Recent research has shown that the coupling of ripples with cortical delta waves and spindles is of particular importance in this memory consolidation process (Maingret et al., 2016).

1.3 The medial septum-diagonal band of Broca regulates theta and sharp wave-ripples

The medial septum-diagonal band of Broca (MS-DB) is another structure in the limbic system that connects to the hippocampus via the fornix. The MS-DB plays a role in both theta rhythms and ripples (Winson, 1978; Vandecasteele et al., 2014).

During theta rhythms, the MS-DB acts as a pacemaker, as lesions of the MS-DB eliminate theta (Winson, 1978; Vandecasteele et al., 2014). In this role, the MS-DB affects both the frequency and amplitude of hippocampal theta rhythms. The various neuron types that make up the MS-DB, however, differ in their individual effects on hippocampal theta.

Parvalbumin-positive GABAergic neurons and cholinergic neurons in the MS-DB receive excitatory input from hypocretin neurons in the lateral hypothalamus (Gerashchenko et al., 2001). GABAergic MS-DB neurons are fast-spiking (Sotty et al., 2003; Mattis et al., 2014). During hippocampal theta, fast GABAergic IPSCs cause synchronous rebound firing in these neurons (Manseau et al., 2008). Firing in these neurons, in turn, is thought to pace hippocampal theta through inhibition of hippocampal inhibitory interneurons at theta frequencies and, thus, disinhibition of hippocampal pyramidal neurons. This process transmits theta rhythmic firing from the septum to the hippocampus (Tóth et al., 1997). Cholinergic MS-DB neurons, on the other hand, tonically depolarize pyramidal and basket neurons in the hippocampus during theta rhythms (Chapman and Lacaille, 1999) and maintain the amplitude, or tone, of hippocampal theta (Kramis et al., 1975; Lee et al., 1994; Gerashchenko et al., 2001; Zhang et al., 2011). Locally, cholinergic MS-DB neurons reciprocally connect to GABAergic and glutamatergic MS-DB neurons (Colom et al., 2005; Leão et al., 2015), and thus may indirectly influence theta rhythms through those connections. The role of glutamatergic neurons in the MS-DB has been the focus of a smaller number of studies (Sotty et al., 2003; Colom et al., 2005), but recent results suggest their involvement in locomotion and theta oscillations as well (Fuhrmann et al., 2015; Justus et al., 2017).

MS-DB neuronal activity also correlates with hippocampal ripples. During ripples, feedback connections from the hippocampus inhibit neural firing in the MS-DB (Alonso and Köhler, 1982; Tóth et al., 1993; Dragoi et al., 1999; Gulyás et al., 2003; Jinno et al., 2007; Takács et al., 2008; Mattis et al., 2014), affecting their role in the septohippocampal circuit. In the hippocamposeptal circuit, fast GABAergic input and

long-lasting hyperpolarizing feedback come from hippocampal somatostatin-positive neurons (Jinno et al., 2007), primarily targeting GABAergic MS-DB neurons and cholinergic MS-DB neurons, respectively (Mattis et al., 2014). Stimulation of hippocamposeptal neurons at 50 Hz, similar to the rate of individual neurons during ripples, evokes long-lasting hyperpolarizing feedback more effectively than stimulation at theta frequency (8 Hz).

Among the different types of neurons in the MS-DB that interact with hippocampal rhythms, cholinergic neurons stand out as a provider of neuromodulation to the hippocampus. The input-output properties of these neurons and how hyperpolarization affects their overall integration properties is not known. Previous work has shown that voltage-gated conductances can change the slope, or gain, of the frequency-current relationship (*f-I* curve) in neurons (Patel and Burdakov, 2015), thus affecting their input-output properties. Therefore, synaptic-mediated hyperpolarization may activate or inactivate voltage-gated conductances and thus affect their gain. Changes in gain could lead to changes in the dynamics of downstream neural circuits. Thus, the bulk of this dissertation focuses on cholinergic neurons in the MS-DB, as well as their potential influences on hippocampal rhythms.

1.4 Physiology of cholinergic neurons in the MS-DB

In vivo, cholinergic MS-DB neurons fire at very slow rates (about 0.5 spikes/s), including during hippocampal theta activity (Simon et al., 2006). *In vitro*, cholinergic MS-DB neurons fire continuously at slightly faster rates (4-10 spikes/s), modulated by mean voltage changes (Griffith and Matthews, 1986; Markram and Segal, 1990). These

neurons also express an inactivating outward current that deinactivates with hyperpolarization and activates with subthreshold depolarization and is identified as a 4-AP sensitive "A-current" (Segal and Barker, 1984; Griffith and Sim, 1990; Markram and Segal, 1990). Activation of this current leads to an increase in the delay to first spike following a current step and has been observed in numerous studies of cholinergic MS-DB neurons (Segal and Barker, 1984; Griffith and Sim, 1990; Markram and Segal, 1990).

This current, which typically inactivates with a time constant of 30 ms (Segal and Barker, 1984), is characterized by a depolarizing notch in membrane voltage following hyperpolarization (Connor and Stevens, 1971; Magariños-Ascone et al., 1999). In other neurons, this current has been shown to enable stable low frequency spike generation (Connor and Stevens, 1971; Connor et al., 1977). Furthermore, previous work has shown that recruitment of the A-current can decrease both the firing rate and the gain in neurons (Connor and Stevens, 1971; Heath et al., 2014; Patel and Burdakov, 2015).

1.5 Cholinergic MS-DB neurons influence hippocampal theta

Stimulation of cholinergic MS-DB neurons enhances low (4-7 Hz), or Type 2, theta power relative to peri-theta frequencies in rodent models (Vandecasteele et al., 2014). Conversely, blockade of only muscarinic acetylcholine (ACh) receptors with atropine leads to attenuation of Type 2, but not Type 1 (7-12 Hz), theta (Kramis et al., 1975; Lawson and Bland, 1993). However, complete elimination of cholinergic MS-DB input to the hippocampus, through procaine injection (Lawson and Bland, 1993) or through lesion by selective immunotoxins (Lee et al., 1994; Gerashchenko et al., 2001), reduces all theta activity. More specifically, lesion of cholinergic MS-DB neurons by 192

immunoglobulin G-saporin results in a decrease in theta power, but not frequency (Lee et al., 1994).

During theta rhythms, cholinergic input from MS-DB neurons to the hippocampus increases (Zhang et al., 2010, 2011), diminishing ripples (Vandecasteele et al., 2014). Although the general size of the effects of ACh on isolated hippocampal neurons is known (Cole and Nicoll, 1983, 1984; Figenschou et al., 1996; Chapman and Lacaille, 1999; McQuiston and Madison, 1999a; Tai et al., 2006), the link between those effects and the suppression of hippocampal ripples is not well established.

The reduction of theta activity through decreases in input from cholinergic MS-DB neurons to the hippocampus also affects learning. Excitotoxic (Leutgeb and Mizumori, 1999) and electrolytic (Winson, 1978) lesions of the septal nuclei cause learning deficits in rats. Immunotoxic lesions of cholinergic neurons in the vertical portion of the diagonal band of Broca (Ridley et al., 1999) and in the basal forebrain (which includes the MS-DB) (Easton et al., 2002) cause learning deficits in monkeys. In humans, blockade of cholinergic receptors in the hippocampus impairs learning and memory (Atri et al., 2004). Cholinergic neuron loss is also implicated in Alzheimer's disease (McGeer et al., 1984), and resulting changes in theta presumably lead to some of the cognitive symptoms associated with Alzheimer's disease (Goutagny and Krantic, 2013). Thus, cholinergic MS-DB neurons are critical for healthy learning and memory function, and their physiological role is of great scientific and medical interest.

1.6 Cholinergic MS-DB neurons influence hippocampal sharp wave-ripples

Cholinergic MS-DB neurons also provide neuromodulation that affects hippocampal ripples. Through optogenetic activation of cholinergic neurons, ripples are suppressed as theta power and coherence are increased (Vandecasteele et al., 2014).

Similar to the effects of ACh on hippocampal rhythms, cholinergic input to hippocampal neurons also causes pronounced effects. In pyramidal neurons, muscarinic input has multiple consequences: membrane voltage and resistance are increased, while spike afterhyperpolarization (AHP) amplitude and spike rate adaptation are decreased (Dodd et al., 1981; Benardo and Prince, 1982; Cole and Nicoll, 1984; Madison and Nicoll, 1984). No major postsynaptic nicotinic response has been found in pyramidal neurons (Frazier et al., 1998), though it is possible ACh has a presynaptic effect (Gray et al., 1996; Zhong et al., 2013). Even so, the muscarinic changes in membrane voltage, membrane resistance, and AHP are likely to have effects on spike output (possibly promoting theta and suppressing ripples).

Cholinergic effects on the interneuron population also include an increase in membrane voltage, though the magnitude of this effect with muscarinic input varies depending on the cell type (Chapman and Lacaille, 1999; McQuiston and Madison, 1999a). Changes in membrane resistance also occur, but depend heavily on interneuron subtype (Chapman and Lacaille, 1999). Interneuron membrane voltage also responds to nicotinic stimulation in varied ways, ranging from nonresponsive to depolarization with diverse timescales (McQuiston and Madison, 1999b).

1.7 Gain changes in cholinergic MS-DB neurons and the mechanism of cholinergic modulation of hippocampal ripples

Understanding the effects of hyperpolarization on the input-output properties of cholinergic MS-DB neurons is crucial to understanding their role in the septohippocampal circuit. In the next chapter, we investigate the effects of hyperpolarization on the input-output properties of cholinergic MS-DB neurons. During this investigation, we found that hyperpolarization caused long-lasting reductions in the firing rate and gain of these neurons. In that chapter we also test the hypothesis that the A-current is responsible for the reduction of neuronal firing rate and gain following hyperpolarization. Contrary to our hypothesis, we observed a 4-AP-insenstive and slowly inactivating K^+ current in cholinergic neurons that reduces the gain.

In Chapter 3, we describe the use of a computational model to investigate the role cholinergic modulation on hippocampal ripples. Specifically, we used the model of ripples to investigate the effects of depolarization on ripple oscillations, finding that imbalances in the drive of the pyramidal neurons and interneurons in the network can disrupt ripples.

In the last chapter, the results of the entire body of work are summarized, and we show how they integrate into the larger research domain of septohippocampal interactions.

CHAPTER 2

GAIN MODULATION OF CHOLINERGIC NEURONS IN THE MEDIAL SEPTUM-DIAGONAL BAND OF BROCA THROUGH HYPERPOLARIZATION

Reprinted with permission from Wiley Periodicals, Inc. Melonakos ED, White JA, Fernandez FR. 2016. Gain modulation of cholinergic neurons in the medial septum-diagonal band of Broca through hyperpolarization. Hippocampus 1541:1525–1541.

HIPPOCAMPUS 26:1525–1541 (2016)

Gain Modulation of Cholinergic Neurons in the Medial Septum-Diagonal Band of Broca Through Hyperpolarization

Eric D. Melonakos,[1]* John A. White,[1,2] and Fernando R. Fernandez[1,2]

ABSTRACT: Hippocampal network oscillations are important for learning and memory. Theta rhythms are involved in attention, navigation, and memory encoding, whereas sharp wave-ripple complexes are involved in memory consolidation. Cholinergic neurons in the medial septum-diagonal band of Broca (MS-DB) influence both types of hippocampal oscillations, promoting theta rhythms and suppressing sharp wave-ripples. They also receive frequency-dependent hyperpolarizing feedback from hippocamposeptal connections, potentially affecting their role as neuromodulators in the septohippocampal circuit. However, little is known about how the integration properties of cholinergic MS-DB neurons change with hyperpolarization. By potentially altering firing behavior in cholinergic neurons, hyperpolarizing feedback from the hippocampal neurons may, in turn, change hippocampal network activity. To study changes in membrane integration properties in cholinergic neurons in response to hyperpolarizing inputs, we used whole-cell patch-clamp recordings targeting genetically labeled, choline acetyltransferase-positive neurons in mouse brain slices. Hyperpolarization of cholinergic MS-DB neurons resulted in a long-lasting decrease in spike firing rate and input-output gain. Additionally, voltage-clamp measures implicated a slowly inactivating, 4-AP-insensitive, outward K^+ conductance. Using a conductance-based model of cholinergic MS-DB neurons, we show that the ability of this conductance to modulate firing rate and gain depends on the expression of an experimentally verified shallow intrinsic spike frequency-voltage relationship. Together, these findings point to a means through which negative feedback from hippocampal neurons can influence the role of cholinergic MS-DB neurons. © 2016 Wiley Periodicals, Inc.

KEY WORDS: spike firing; voltage-gated K^+ conductance; exponential integrate-and-fire model; acetylcholine; electrophysiology

This article was published online on September 15, 2016. After online publication text corrections were made. This notice is included in the online and print versions to indicate that both have been corrected on September 24, 2016.

[1] **Department of Bioengineering, University of Utah, Salt Lake City, Utah;** [2] **Department of Biomedical Engineering, Boston University, Boston, Massachusetts**

Grant sponsor: NIH; Grant number: R01MH085074; Grant sponsor: NIH; Grant number: R03MH103728.

Abbreviations used: MS-DB, medial septum-diagonal band of Broca; SPW-R, sharp wave-ripple; *f-I* curve, frequency-current curve; $ChAT^+$, choline acetyltransferase-positive; *f-V* curve, frequency-voltage curve; ACSF, artificial cerebrospinal fluid; AHP, afterhyperpolarization; *I-V*, current-voltage; 4-AP, 4-aminopyridine; eLIF, exponential leaky integrate-and-fire; LIF, leaky integrate-and-fire; I_{siK}, slowly inactivating K^+ current; SD, standard deviation.

*Correspondence to: Eric D. Melonakos, Department of Bioengineering, University of Utah, 36 Wasatch Drive, Salt Lake City, UT 84112. E-mail: eric.melonakos@gmail.com

Accepted for publication 30 August 2016.
DOI 10.1002/hipo.22653
Published online 2 September 2016 in Wiley Online Library (wileyonlinelibrary.com).

INTRODUCTION

Hippocampal electrical oscillations are thought to be critical for information processing. For example, theta rhythms (4 − 12 Hz) are correlated with attention, navigation, and memory encoding (Berry and Thompson, 1978; Winson, 1978; see Buzsáki, 2005, for review; Hasselmo, 2005), whereas sharp wave-ripple complexes (SPW-Rs; 140 − 220 Hz) are important for memory consolidation (Girardeau et al., 2009). Both rhythms are influenced by the medial septum-diagonal band of Broca (MS-DB) (Winson, 1978; Vandecasteele et al., 2014), which contains GABAergic, cholinergic, and glutamatergic neurons and innervates the hippocampus via the fornix.

During theta rhythms, cholinergic MS-DB neurons are thought to tonically depolarize pyramidal and basket neurons in the hippocampus (Chapman and Lacaille, 1999), and are responsible for maintaining theta amplitude (Kramis et al., 1975; Lee et al., 1994; Gerashchenko et al., 2001; Zhang et al., 2011), while at the same time attenuating hippocampal SPW-Rs (Vandecasteele et al., 2014). During SPW-Rs, MS-DB neuron firing is suppressed (Dragoi et al., 1999). The source of this suppression is most likely feedback connections from the hippocampus (Alonso and Köhler, 1982) which provide inhibitory input to MS-DB neurons (Tóth et al., 1993; Jinno et al., 2007; Takács et al., 2008). This inhibitory feedback includes both fast GABAergic input from somatostatin-positive neurons (Jinno et al., 2007), primarily targeting GABAergic MS-DB neurons, and long-lasting hyperpolarizing feedback, primarily targeting cholinergic MS-DB neurons (Mattis et al., 2014). The long-lasting hyperpolarizing feedback is evoked most effectively following SPW-R frequency stimulation (as opposed to theta frequency stimulation) of hippocamposeptal neurons. This may point to a functional link between cholinergic neuron membrane voltage modulation and hippocampal network oscillation frequency. By altering firing behavior in cholinergic neurons, hyperpolarizing feedback from the hippocampus to cholinergic neurons may, in turn, change hippocampal network activity. However, little is known about the integration properties of cholinergic neurons in the MS-DB and how hyperpolarization affects the overall integration properties in these neurons.

Hyperpolarization of cholinergic neurons could deinactivate an "A-current", a K^+ current previously shown to be expressed in these neurons (Segal and Barker, 1984; Griffith and Sim, 1990; Markram and Segal, 1990). Furthermore, previous work has shown that recruitment of an A-current can decrease both the overall spike firing rate as well as the slope, or gain, of the frequency-current relationship (*f-I* curve) in neurons (Connor and Stevens, 1971; Heath et al., 2014; Patel and Burdakov, 2015). We hypothesized that hyperpolarization of MS-DB neurons may allow for activation of voltage-gated K^+ conductances consistent with an A-current and fundamentally alter the integration properties and spike output characteristics of cholinergic neurons.

Using whole-cell patch-clamp in mouse brain slices and targeting genetically labeled choline acetyltransferase-positive ($ChAT^+$) neurons, we show that hyperpolarization of cholinergic MS-DB neurons results in a long-lasting decrease in firing rate and gain. Additionally, our results indicate that a slowly inactivating, 4-AP-insensitive, outward K^+ conductance, distinct from the A-current, is responsible. Finally, we demonstrate that the modulation of firing rate and gain through hyperpolarization and recruitment of a K^+ current depends on the expression of a shallow spike frequency-voltage relationship (*f-V* curve). Together, these findings show that hyperpolarization alters the integrative properties of cholinergic MS-DB neurons, reducing their firing rate and gain, through the recruitment of a slowly inactivating K^+ conductance.

MATERIALS AND METHODS

All of the University of Utah Institutional Animal Care and Use Committee guidelines and provisions were followed.

Tissue Preparation

To create mice in which we could identify cholinergic neurons, we crossed ChAT-IRES-Cre knockin mice (B6;129S6-*Chat*$^{tm2(cre)Lowl}$/J, stock number 006410; Jackson Labs) with Ai9 mice possessing a loxP-flanked STOP cassette hindering transcription of tdTomato (B6;129S6-*Gt(ROSA)26Sor*$^{tm9(CAG-tdTomato)Hze}$/J, stock number 007905; Jackson Labs). From the resulting progeny of this crossing, we prepared coronal slices of the MS-DB from 54 mice (23 − 251 days old) of either sex. All chemicals were obtained from Sigma-Aldrich unless otherwise noted. Mice were anesthetized using isoflurane and decapitated, after which brains were removed and submersed in 0°C artificial cerebrospinal fluid (ACSF). Both slicing and recording ACSF solutions contained (in mM): 125 NaCl, 25 $NaHCO_3$, 25 D-glucose, 2.5 KCl, 2 $CaCl_2$, 1.25 NaH_2PO_4, and 1 $MgCl_2$, buffered to a pH of 7.4 using 95% O_2/5% CO_2. Immediately following submersion in ACSF, brains were sectioned using a vibratome (Leica VT1000 S; Leica Biosystems) into 400-µm slices. Following sectioning, slices were transferred to an incubation chamber at 30°C for 20 min, after which the incubation chamber was cooled to room temperature (20°C). At the time of experiments, slices were transferred to a perfusion chamber under a microscope (Axioscope 2+; Zeiss) equipped to excite and visualize tdTomato fluorescence (excitation: 554 nm; emission: 581 nm). Each slice contained numerous fluorescing neurons, from which healthy ones were selected for electrophysiological recordings. The perfusion chamber temperature during recordings was between 32 and 34°C.

Electrophysiology

Recording micropipettes were drawn on a micropipette puller (P-97; Sutter Instruments) and filled with intracellular fluid comprised of (in mM): 136 K-gluconate, 4 KCl, 10 HEPES, 7 diTrisPhCr, 4 Na_2ATP, 2 $MgCl_2$, 0.3 Tris-GTP, and 0.2 EGTA, buffered to a pH of 7.4 using KOH. Electrophysiological experiments were completed using a MultiClamp 700B amplifier (Molecular Devices), and data was acquired using the Real-Time eXperiment Interface (Lin et al., 2010) at a sample rate of 10 kHz. Typical pipette resistance was 3 − 5 MΩ, and typical series resistance was 15 − 60 MΩ. Although relatively high, the series resistance during voltage-clamp experiments was sufficient to measure the presence and approximate size and kinetics of the slowly inactivating current (measurements ranged from −3.3 to 6.3 nA). We also compensated for series resistance using the Rs Compensation tool available in the MultiClamp 700B software (Bandwidth = 1.02 kHz, Correction = 50 − 80%). The perfusion ACSF for most experiments contained 10 µM DNQX and 50 µM picrotoxin to eliminate voltage fluctuations arising from synaptic activity.

Simulations

We used Matlab (R2011a; MathWorks) for all model simulations, and each model was solved using the forward Euler method with a time step of 0.01 ms. The membrane voltage of the model was governed by the following equation:

$$C\frac{dV}{dt} = -g_L(V-E_L)+g_L\Delta_T\exp\left(\frac{V-V_{th}}{\Delta_T}\right) - g_{siK}bh(V-E_{siK})-I_w+I_e+I_{noise},$$

where C is the membrane capacitance (81.9 pF), V is the membrane voltage, g_L is the leak conductance (1.3 nS), E_L is the leak reversal (−85 mV), Δ_T is the spike slope factor (2 mV default), V_{th} is the threshold voltage (−59.5 mV), g_{siK} is the slowly inactivating, outward K^+ conductance (30.1 nS maximum), b is the K^+ conductance activation, h is the K^+ conductance inactivation, E_{siK} is the K^+ reversal potential (−93.1 mV), I_w is the spike-dependent adaptation current, I_e is the input current, and I_{noise} is the noise current.

Equations governing the various currents are as follows:

$$\frac{dI_w}{dt} = \frac{g_w(V-E_L)-I_w}{\tau_w}$$

(spike−dependent adaptation current;

g_w = 0.1 nS, τ_w = 125 ms, each spike adds 2.5 pA to I_w)

$$\frac{db}{dt} = \frac{b_\infty - b}{\tau_b}$$
$$\left(K^+ \text{conductance activation}; \tau_b = 152.7 \text{ ms}\right)$$
$$\frac{dh}{dt} = \frac{h_\infty - h}{\tau_h}$$
$$\left(K^+ \text{conductance inactivation}; \tau_h = 11100 \text{ ms}\right)$$
$$b_\infty = 0.14 + \frac{0.81}{1+\exp\left(\frac{-22.46-V}{8.08}\right)}$$
$$\left(K^+ \text{conductance steady-state activation}\right)$$
$$h_\infty = 0.08 + \frac{0.88}{1+\exp\left(\frac{-60.23-V}{-5.69}\right)}$$
$$\left(K^+ \text{conductance steady-state inactivation}\right)$$

Following a threshold crossing of 0 mV, voltage was reset to −65 mV. We also added a current noise term, I_{noise}, in order to account for small membrane voltage fluctuations seen in the absence of any synaptic input. I_{noise} was generated using white noise that is low-pass filtered [100 Hz cutoff frequency (f_{cut})]. Noise signals were first constructed in the frequency domain using the frequency amplitude [$A(f)$] equation $A(f) = \sqrt{\frac{1}{(2\pi f_{cut})^2 + (2\pi f)^2}}$, and then converted into time series using Matlab's *ifft* function. The standard deviation of the simulated voltage with noise was 0.6 ± 0.0006 mV at -79.5 ± 0.0009 mV for $\Delta_T = 2$ mV and 0.7 ± 0.0006 mV at -79.1 ± 0.001 mV for $\Delta_T = 10$ mV. The membrane resistance was 190.5 ± 1.1 MΩ for $\Delta_T = 2$ mV and 196.1 ± 1.1 MΩ for $\Delta_T = 10$ mV.

Data Analysis

All values and error bars are reported as mean ± SEM. Statistical tests were performed using an α-level of $P = 0.05$ unless otherwise noted. Data analyses were performed using custom and built-in functions in Matlab. Input resistances, membrane capacitances, and membrane time constants were all extracted in current-clamp mode from current steps that elicited a subthreshold voltage change of 5 − 10 mV. Resting voltage was the average membrane potential while the current was held at 0 pA for 2 s. Spike frequency was calculated by counting spikes and dividing by the current step duration. Gain was calculated by linear regression analysis using Matlab's *regstats* function in the statistical toolbox. For both experimental and modeling gains, lines were fitted to all currents from threshold (i.e., firing rate > 0 spikes/s) to the first current step with the maximum firing rate. In many of the cases following hyperpolarization, the linear fits of the *f-I* curves had a low R^2 value, owing to the narrow dynamic range and few spike frequency data points. In these cases, fit accuracy was visually confirmed. During some experiments, current-based artificial synaptic noise was added using an Ornstein-Uhlenbeck process, as described in Fernandez et al. (2011), with a mean current of 0 pA, time constant of 10 ms, and SD of 20 − 30 pA.

For firing rate vs. time analyses, firing rate was calculated using a 3 s binning window that moved forward in 0.3 s steps. The depth (amplitude) of the afterhyperpolarization (AHP) was measured as the difference between the voltage at the threshold of the spike (the time of the maximum second derivative of the spike) and the minimum voltage during the AHP of the spike. AHP duration was defined as the time between crossing the spike threshold voltage on the downstroke and when the voltage recovered to 40% of its value relative to threshold. In order to get accurate measurements of AHP depth, AHPs were only measured for spikes that occurred before the last 0.05 s of the current pulse. We first averaged AHP measurements within each current pulse and then binned the average AHP measurements from different current pulses by spike firing rate.

For voltage-clamp data, baseline currents were zeroed offline, and leak currents were subtracted either manually using a linear fit of the subthreshold current-voltage (*I-V*) curve (for reversal potential experiments) or automatically using the MultiClamp 700B software (for activation and inactivation curve experiments). To determine the reversal potential of the slowly inactivating current, we calculated the x-intercept of the tail current-voltage curve found by stepping to a range of voltages following activation of the conductance. Although the voltage range and step size varied between trials [e.g. (in mV) −50 to −100, −60 to −110, and −50 to −125 in 5 mV steps; −65 to −72.5, −65 to −100, −65 to −90, and −65 to −85 in 2.5 mV steps], the reversal potential for each trial was calculated individually.

In our analysis of the activation and inactivation curves, conductance was calculated using $g = I/(V-E)$, with the reversal $E = -93.1$ mV. Activation and inactivation curves were fit using the sigmoidal function $f(V) = a + b \Big/ \left(1+\exp\left(\frac{V_{1/2}-V}{k}\right)\right)$, where $V_{1/2}$ is the midpoint of the sigmoid, k is the slope, b is the maximum of the curve minus the offset, and a is the offset of the curve. For *I-V* curves, we measured the average subthreshold or suprathreshold interspike voltage in response to current steps in current-clamp mode. Suprathreshold interspike voltages were measured during the time between the end of the spike AHP (as defined above) and the inflection point of the next spike. For these and the *f-V* curves, the first 250 ms of the pulse was excluded from the voltage average to allow voltage to reach a steady-state. In one case, the voltage during an interspike interval was not included in the analysis due to the interspike interval occurring during the last 0.05 s of its current pulse. Resistance curves were derived from *I-V* curves by using running linear regressions of the *I-V* curves, with lines fitted to 15 pA windows that moved forward in 5 pA steps. The slope of each linear regression was taken to be the resistance at the average voltage over the fitted points. Resistances were then binned into 10 mV voltage bins. Average membrane voltage for the *f-V* curves included spikes.

The drugs 4-aminopyridine (4-AP; Sigma-Aldrich), hongotoxin-1 (Alomone Labs), XE991 (Tocris Bioscience), and

tetraethylammonium (TEA; Sigma-Aldrich) were added to the ACSF at appropriate concentrations during the experiments as indicated below.

RESULTS

Hyperpolarization Reduces Firing Rate and Gain in Cholinergic MS-DB Neurons

To address how hyperpolarization alters the integration properties of cholinergic neurons, we used brain slices of the MS-DB and specifically targeted cholinergic neurons using transgenic mice with Cre-dependent expression of the red fluorescent protein variant tdTomato in $ChAT^{+}$ neurons (Fig. 1A). For comparisons, we also made electrophysiological measures from non-cholinergic (non-fluorescent) neurons, the majority of which were fast-spiking, and likely GABAergic (Sotty et al., 2003; Mattis et al., 2014).

Initial characterization indicated that input resistance, membrane capacitance, and membrane time constant values were not significantly different between cholinergic neurons and non-cholinergic neurons at -77.8 ± 0.0002 mV (cholinergic vs. non-cholinergic: 350.4 ± 30.4 MΩ vs. 347.7 ± 52.3 MΩ; 81.9 ± 5.7 pF vs. 66.7 ± 15.1 pF; and 26.9 ± 2.2 ms vs. 25.5 ± 10.9 ms, respectively) (Fig. 1B; $0.964 \geq P \geq 0.252$, two-tailed unpaired *t*-tests; $n = 30$ cholinergic neurons vs. 11 noncholinergic neurons). Resting voltage for most cholinergic neurons was above spike threshold (-45.6 ± 1.5 mV; $n = 13$). To assess the impact of hyperpolarization on cholinergic neuron spike firing output, we started by hyperpolarizing neurons and quantifying the effect on the subsequent spike firing rate. In current-clamp mode, we held neurons at depolarized potentials (-43.0 ± 1.8 mV). We then delivered current pulses of varying magnitudes (-55 to -300 pA) in order to transiently hyperpolarize membrane voltage to -72.5 ± 2.0 mV for 0.5 s. Upon release from hyperpolarization, we measured the firing rate during the subsequent 4.5 s. We repeated this protocol for 24 pulses and averaged the firing rates over the pulses. For control experiments, neurons were held at depolarized (i.e., non-hyperpolarized) voltages (-44.0 ± 1.7 mV) before measuring firing rate. In cholinergic neurons, we observed that brief, hyperpolarizing current pulses led to a significant reduction in mean firing rate, with a >40% reduction in firing rate when normalized to the average control firing rate (Figs. 1Cii and 1Ciii; 1.6 ± 0.4 spikes/s compared to control rates of 2.9 ± 0.4 spikes/s; $P = 0.006$ for raw rates and 0.004 for normalized rates, two-tailed paired *t*-tests; $n = 12$). In contrast, in noncholinergic MS-DB neurons, hyperpolarization to -71.8 ± 2.3 mV evoked a non-significant increase in firing rate over control (-51.8 ± 3.3 mV) (Figs. 1Dii and 1Diii; 2.4 ± 0.4 spikes/s compared to control rates of 2.1 ± 0.4 spikes/s; $P = 0.376$ for raw rates and 0.197 for normalized rates, two-tailed paired *t*-tests; $n = 13$ and 12, respectively).

Given that brief bouts of hyperpolarization reduced the firing rate in cholinergic neurons, we were also interested to know if hyperpolarization could modulate the overall scaling of the input-output relationship and provide a mechanism of gain control in these neurons. To quantify the gain, we used the slope of the *f-I* curve. We measured the *f-I* curves of cholinergic MS-DB neurons using 5 s currents over a 200 pA range, delivered in 10 pA steps. Each current pulse in the series followed either 1 s hyperpolarization (-81.5 ± 0.3 mV) or depolarization (-50.8 ± 0.6 mV). Spike rheobase did not change significantly following hyperpolarization (96.8 ± 8.4 pA following hyperpolarization vs. 95.5 ± 7.9 pA following depolarization; $P = 0.0546$, two-tailed paired *t*-test; $n = 31$). However, we found that current pulses following hyperpolarization not only led to a reduction in firing rate compared to those following depolarization, but also led to a 0.5 ± 0.1-fold divisive (reduction in gain) effect on the *f-I* curve, reducing the mean gain from 37.8 ± 4.5 spikes/nA·s following depolarization to 19.5 ± 4.6 spikes/nA·s following hyperpolarization (Fig. 2Aiii, inset; $P < 0.001$, two-tailed paired *t*-test; $n = 30$). Conversely, non-cholinergic MS-DB neurons exhibited no significant difference between hyperpolarized (-82.1 ± 0.3 mV) and depolarized (-49.9 ± 0.9 mV) conditions, with gains of 211.1 ± 60.2 spikes/nA·s and 262.8 ± 57.1 spikes/nA·s, respectively (Fig. 2Biii, inset; $P = 0.192$, two-tailed paired *t*-test; $n = 10$). Thus, hyperpolarization, or the membrane voltage history, selectively modulates both the mean and scaling of spike output in cholinergic neurons.

Synaptic inputs present *in vivo* cause large membrane voltage fluctuations (Paré et al., 1998; Anderson et al., 2000). Synaptic fluctuations, or synaptic noise, can cause changes in neuronal gain (Fernandez et al., 2011). In order to observe the size of the gain reduction during noisy, *in vivo*-like conditions, we added artificial synaptic noise using an Ornstein-Uhlenbeck process (see Methods). We found that the gain reduction persisted under noisy conditions, with gains of 30.2 ± 3.5 spikes/nA·s following hyperpolarization and 50.3 ± 7.2 spikes/nA·s following depolarization (Fig. 2Ciii, inset; $P = 0.0002$, two-tailed paired *t*-test; $n = 18$), suggesting that *in vivo* membrane voltage fluctuations do not preclude the effect.

Voltage Dependence, Time Dependence, and Recovery Time of Hyperpolarization-Induced Firing Rate Reduction

To better quantify the hyperpolarization-induced reduction in firing rate we observed and to assess the dependence of the effect on the duration and amplitude of cholinergic neuron hyperpolarization, we further characterized the phenomenon in three different ways: the (1) voltage dependence, (2) time dependence, and (3) recovery time of the effect.

As shown in Figure 3A, the reduction of firing rate was induced gradually and became significantly larger with increasing hyperpolarization (Fig. 3Aii; $P = 0.003$; one-way ANOVA between the mean firing rates for the first 3 s following each hyperpolarization level; $n = 2$ to 7 neurons). The largest decrease in firing rate occurred as the membrane voltage was hyperpolarized to voltages below -60 mV prior to eliciting spike discharge ($P < 0.001$ for

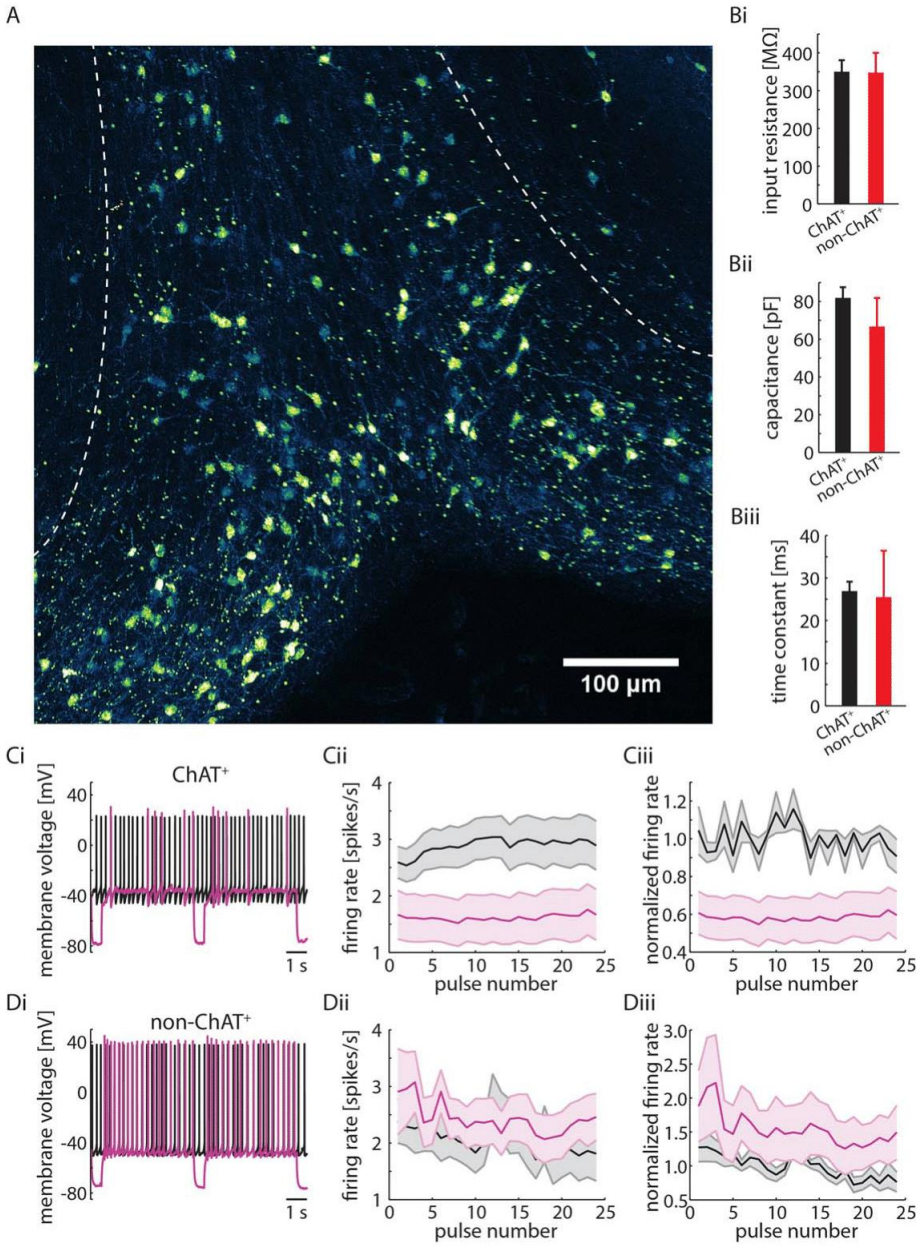

FIGURE 1. Hyperpolarization of cholinergic MS-DB neurons caused a reduction in firing rate. A: ChAT$^+$ neurons (green false color) in the MS-DB were identified using the transgenic expression of the fluorescent marker tdTomato. Dotted lines delineate approximate MS-DB boundaries. B: There were no significant differences between input resistance (*i*), membrane capacitance (*ii*), and membrane time constant (*iii*) values for ChAT$^+$ and non-ChAT$^+$ neurons. C: Brief hyperpolarization of ChAT$^+$ neurons to −72.5 mV resulted in a reduction in firing rate, as shown in an example (*i*), in averaged firing rates (*ii*), and in averaged normalized firing rates (*iii*). For C and D, data from hyperpolarizing pulses are shown in purple for visualization purposes. Throughout subsequent figures, gray lines indicate hyperpolarized data and black lines indicate depolarized data, unless otherwise specified. D: Hyperpolarization of non-ChAT$^+$ neurons to −71.8 mV did not result in a reduced firing rate and even led to non-significant increases in firing, as shown in an example (*i*), in averaged firing rates (*ii*), and in averaged normalized firing rates (*iii*). [Color figure can be viewed at wileyonlinelibrary.com]

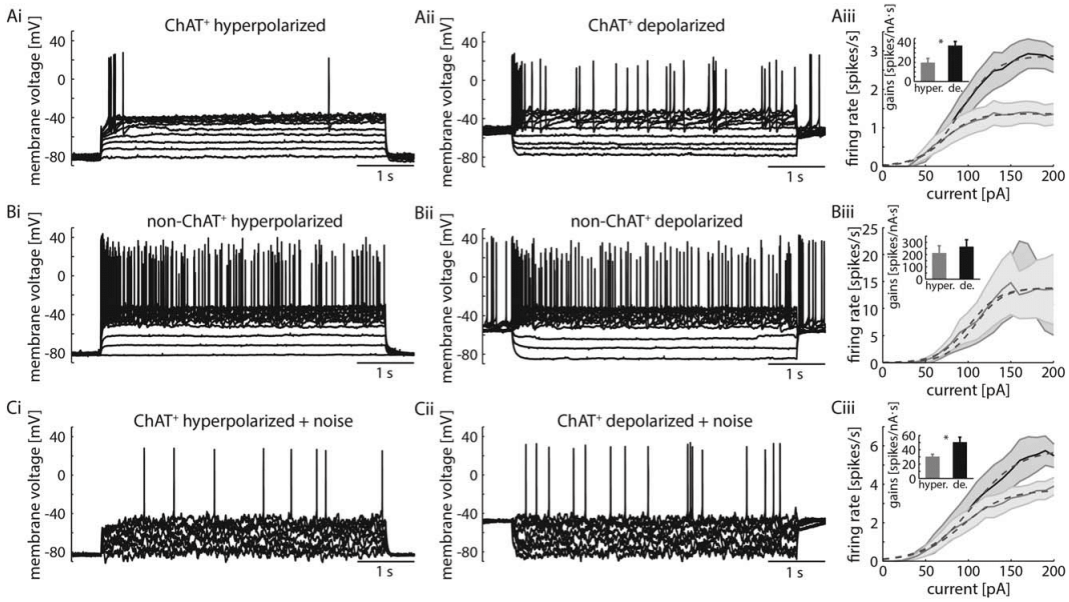

FIGURE 2. Hyperpolarization of cholinergic MS-DB neurons caused a divisive effect on the *f-I* curve. A: Hyperpolarization of a ChAT$^+$ neuron led to a divisive effect on the *f-I* curve. The sensitivity of the neuron to input currents following hyperpolarization (*i*) was less than that following depolarization (*ii*), as shown in the average *f-I* curve (*iii*). The average slope (gain) of the *f-I* curve is shown in A*iii*, *inset*. B: Hyperpolarization of non-ChAT$^+$ neurons had no significant effect on the *f-I* curve, as seen in examples *i* and *ii* and in the average *f-I* curve (*iii*). In these neurons, the gain (*iii*, *inset*) did not change in a voltage-history dependent manner. C: Hyperpolarization continued to significantly reduce gain in the presence of artificial synaptic noise (*iii*, *inset*). Sigmoidal fits of average *f-I* curves in A*iii*, B*iii*, and C*iii* (dashed lines) are for visualization purposes only.

comparison between hyperpolarization from −70 mV to −60 mV and hyperpolarization from −50 to −40 mV, $n = 6$ and 7, respectively; $P = 0.002$ for comparison between hyperpolarization from −70 mV to −60 mV and hyperpolarization from −40 mV and −30 mV, $n = 6$ and 2, respectively; $\alpha = 0.0083$, two-tailed unpaired *t*-tests). Likewise, greater durations in hyperpolarization increased the magnitude and time of the firing rate reduction (Fig. 3Bii; $P < 0.001$, one-way ANOVA between the mean firing rates for the first 3 s following each hyperpolarization time length; $n = 7$ neurons). Increasing hyperpolarization time from 0.05 s to 0.5 s (at -81.0 ± 1.1 mV) resulted in a significant decrease in firing rate ($P = 0.0006$; $\alpha = 0.0083$, two-tailed paired *t*-tests; $n = 7$ neurons). Further lengthening hyperpolarization time to 5 s did not result in a significant additional decrease in firing rate.

Next, we hyperpolarized neurons to -95.3 ± 3.9 mV for 10 s in order to quantify the amount of time it took cholinergic MS-DB neurons to recover to baseline firing rates after strong activation of the hyperpolarization-induced slowing of firing. We saw recovery to near-baseline rates after 60 s (Fig. 3Cii; $n = 7$). By fitting an exponential function to the firing rate following hyperpolarization, we found that recovery had an average time constant of 9.2 ± 3.3 s. Thus, hyperpolarization induces a reduction in subsequent firing rate that can last tens of seconds. Together, these findings show that cholinergic neurons, unlike other neurons in the MS-DB, reduce their firing rates for extremely long periods of time in response to relative short periods of hyperpolarization.

4-AP-Sensitive Currents Are Not Responsible for Hyperpolarization-Mediated Changes in Input-Output Properties

Fast-inactivating K^+ currents that activate and inactivate at subthreshold membrane voltages, known as "A-currents", lead to a delay to first spike (Segal and Barker, 1984) similar to that observed at the beginning of our traces from cholinergic neurons following hyperpolarization (e.g. in Fig. 2Ai). In addition, we observed a depolarizing notch in membrane voltage following hyperpolarization, which has also been observed in neurons that express an A-current (Connor and Stevens, 1971; Magariños-Ascone et al., 1999) (Fig. 4Bi, inset). Further, this current has been observed in other studies of cholinergic MS-DB neurons (Griffith and Sim, 1990; Markram and Segal, 1990). Because of its deinactivation with hyperpolarization, we hypothesized that an A-current could be responsible for the reduction in firing rate and gain through an increase in outward current following hyperpolarization.

To determine the involvement of an A-current in the gain reduction we observed, we bath applied 10 mM 4-aminopyridine (4-AP), a drug that blocks the K^+ channels that generate an A-current, among other currents. When 4-AP was added, the

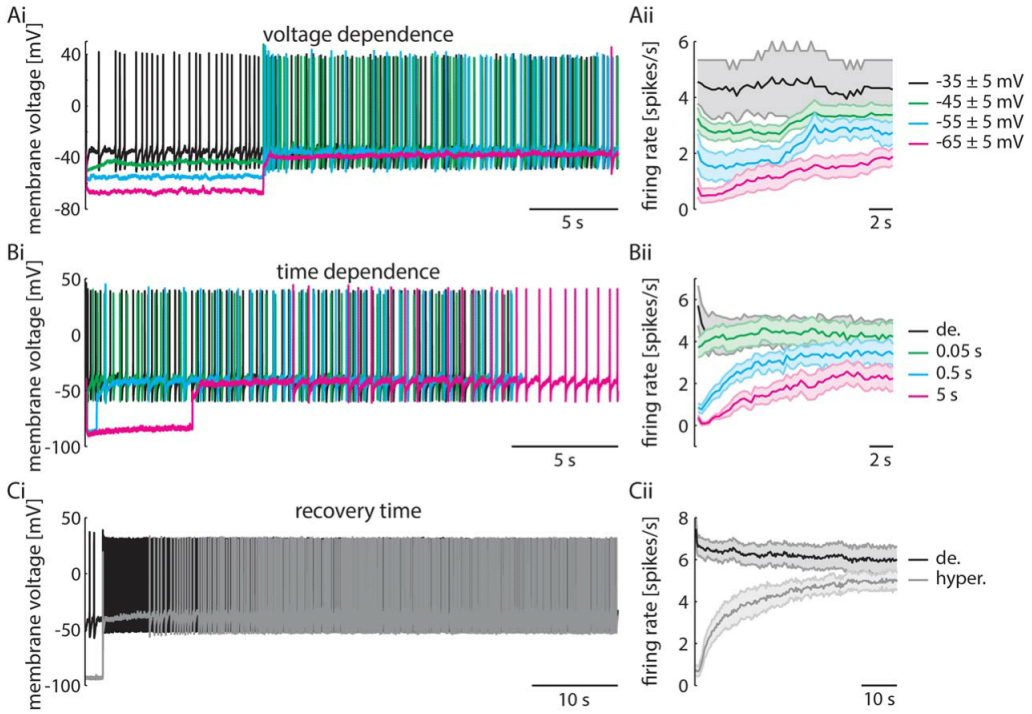

FIGURE 3. Characterization of the voltage dependence, time dependence, and recovery time of the hyperpolarization-induced firing rate reduction. A: Firing rate decreased during pulses following hyperpolarization as the level of hyperpolarization increased, as shown in example traces (*i*) and in averaged data (*ii*) for −30 to −40 mV ($n = 2$), −40 to −50 mV ($n = 7$), −50 to −60 mV ($n = 7$), and −60 to −70 mV ($n = 6$). B: Hyperpolarization to −81.0 mV for at least 0.5 s was necessary before firing rate reductions became significant, as shown in example traces (*i*) and averaged data (*ii*). Greater levels (A) and time lengths (B) of hyperpolarization led to progressively larger reductions in firing rate. C: Following strong activation of the effect, firing rates recovered to near-baseline values with a time constant of 9.2 s, as shown in example traces (*i*) and averaged data (*ii*). [Color figure can be viewed at wileyonlinelibrary.com]

characteristic notch in membrane voltage disappeared (Fig. 4Bii, inset) and the delay to first spike following hyperpolarization was reduced from an average of 450.3 ± 55.8 ms to 42.4 ± 7.0 ms (Figs. 4Bi and 4Bii; $P < 0.001$, two-way ANOVA; $n = 31$ neurons without 4-AP and 5 neurons with 4-AP). Despite the elimination of the delay and membrane voltage notch, the reduction in gain following hyperpolarization remained in the presence of 10 mM 4-AP, with gain decreasing from 44.1 ± 4.8 spikes/nA·s to 19.4 ± 8.0 spikes/nA·s following a 1 s long hyperpolarization to −81.2 ± 0.8 mV (Fig. 4C, inset; $P = 0.017$, two-tailed paired *t*-test; $n = 5$). Thus, although the A-current is responsible for the delay to first spike and the membrane notch following hyperpolarization, it is not responsible for the reduction in gain following hyperpolarization in cholinergic MS-DB neurons.

Cholinergic MS-DB Neurons Express a Slowly Activating and Inactivating, Voltage-Gated K^+ Current

Consistent with the lack of effect of 4-AP on firing rate and gain following hyperpolarization, A-currents typically inactivate with a time constant of less than 100 ms (Segal and Barker, 1984; Zona et al., 1988; Griffith and Sim, 1990; Bekkers, 2000), a time frame too short to account for the effects of hyperpolarization on cholinergic neurons. For this reason, we hypothesized that an outward K^+ current that is deinactivated by hyperpolarization, but with activation and inactivation kinetics much slower than a typical A-current, could be responsible for the changes in firing rate and gain. To determine the presence of this current, we performed voltage-clamp experiments with bath applied 10 mM 4-AP and 500 nM TTX. Note that we confirmed the presence of the A-current in voltage-clamp and eliminated it from our recordings with 4-AP (see Figs. 5Bi and 5Bii for sample recordings without and with 4-AP, respectively).

In voltage-clamp, we observed a large and slowly inactivating outward current in response to a depolarizing step to 0 mV from a holding voltage of −80 mV (Figs. 5Ai and 5Aii). To calculate the reversal potential of the current, we hyperpolarized to −80 mV for 30 s to deinactivate the channels, followed by depolarizing to −30 mV for 5 s, which was then followed by a step ranging from −50 to −125 mV (see Methods).

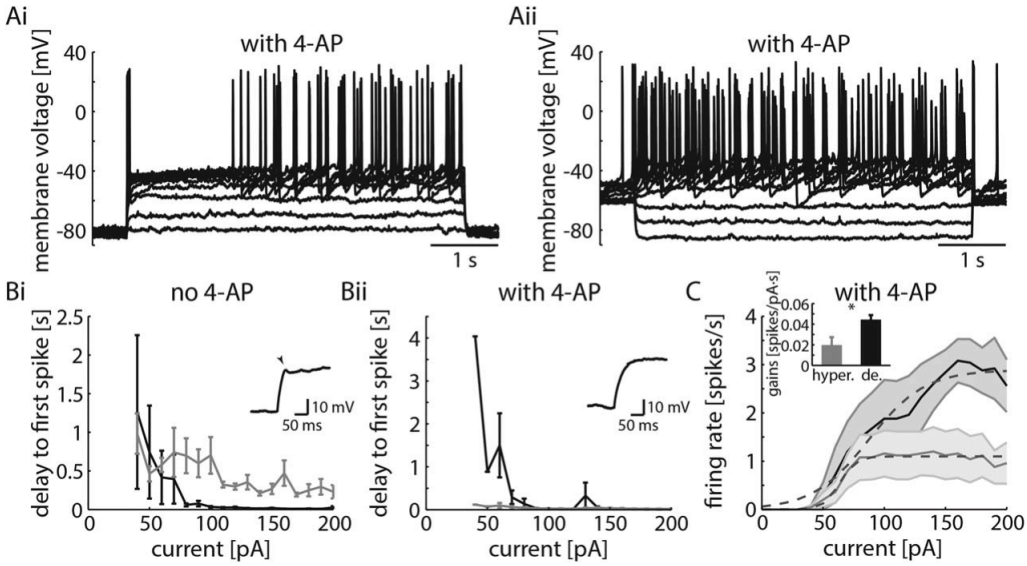

FIGURE 4. 4-AP-sensitive currents were not responsible for the divisive change in the *f-I* curve. A: Example traces of a cholinergic neuron with bath applied 10 mM 4-AP following hyperpolarization (*i*) and depolarization (*ii*). B: The presence of a delay to first spike following hyperpolarization (*i*), as well as the distinctive notch (arrowhead) and non-exponential charging curve (*i*, *inset*), resulted from the presence of an A-current in cholinergic MS-DB neurons without 4-AP. The delay (*ii*), non-exponential charging curve, and notch (*ii*, *inset*) were successfully eliminated following application of 4-AP. C: Average *f-I* curves with 4-AP indicated that the A-current was not responsible for the reduction in gain following hyperpolarization. Sigmoidal fits of average *f-I* curves (dashed lines) are for visualization purposes only.

During the range of steps, we measured a tail current that reversed at -93.1 ± 6.3 mV, which is consistent with a K^+ current ($n = 11$). Further, the maximum conductance was 34.1 ± 9.3 nS, indicating a relatively large K^+ conductance with the potential to significantly influence excitability (Fig. 5Ci; $n = 5$). The conductance began inactivating around -70 mV and was >80% inactivated around -40 mV, leaving a window conductance of 1.8 ± 0.7 nS at -44.3 ± 0.9 mV (i.e. an overlap between activation and inactivation curves) (Fig. 5Cii; $n = 5$). Each activation and inactivation curve was fit with a sigmoid, from which the midpoint ($V_{1/2}$) and slope (k) were extracted. The $V_{1/2}$ of activation for the K^+ current was -22.5 ± 1.3 mV, and the k was 8.1 ± 3.6 mV (Fig. 5Cii; $n = 5$), while the $V_{1/2}$ of inactivation was -60.2 ± 1.0 mV, and the k was -5.7 ± 1.1 mV (Fig. 5Cii; $n = 5$). The time constants of activation and inactivation were 152.7 ± 19.2 ms (a range of 9.3 ms to 575.1 ms) and 11.1 ± 1.6 s (a range of 3.3 s to 55.4 s), respectively ($n = 5$ for activation and 4 for inactivation). Our attempts to find a specific blocker of the current with various drugs, including the K^+ channel blockers 4-AP (10 mM), Hongotoxin-1 (10 nM), and XE991 (20 μM), were not successful. We did, however, discover that blocking the current was possible with 20 mM TEA. Because TEA simultaneously blocked K^+ channels crucial for normal action potential repolarization, we could not ascertain the involvement of the slow K^+ current in reducing firing rate and gain using a pharmacological approach.

As indicated, activation of the K^+ conductance occurred in the suprathreshold voltage region. To confirm this in current-clamp, we measured the subthreshold *I-V* curves following hyperpolarization and depolarization. From this, we derived the subthreshold membrane input resistance curves by taking the slopes of a running linear fit of the *I-V* curves (see Methods). The *I-V* curves showed little difference following hyperpolarization and depolarization (Fig. 5Di; $P = 0.0425$, two-way ANOVA; $n = 35$ neurons), with no significant difference in membrane input resistance across the entire subthreshold voltage region (Fig. 5Dii; $P = 0.7168$, two-way ANOVA; $n = 35$ neurons). These results confirm that any differences that could lead to changes in firing rate or gain are the result of the K^+ conductance activation in the suprathreshold voltage region.

Reduced Firing Rate and Gain Is Associated with Minimal Changes in Spike Shape

Next, we sought to understand how the slowly inactivating K^+ current reduced firing rate and gain. The change in firing rate and current threshold is easily explained by the hyperpolarizing current associated with recruiting K^+ currents at or near spike threshold. The reduction in gain, however, is more difficult to explain due to the slow kinetics of the K^+ current we observed in voltage-clamp. Often, reducing the gain of a neuron requires a current that activates within the time-frame of a spike and is able to significantly influence spike parameters,

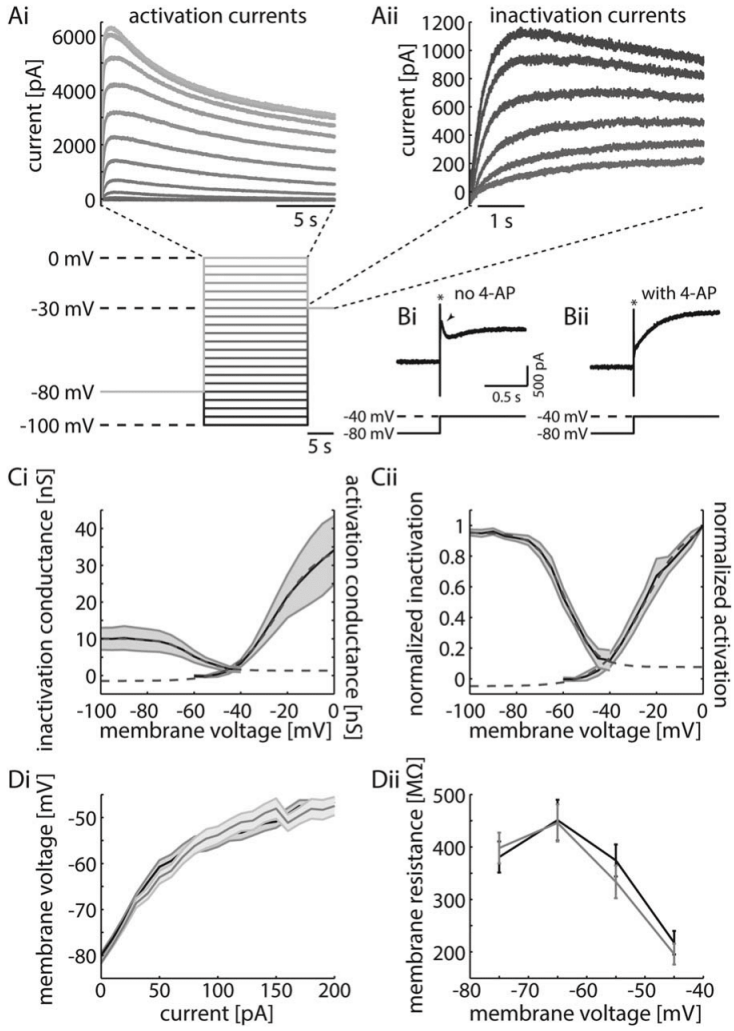

FIGURE 5. Voltage-clamp measures revealed the presence of a slow inactivating, outward current. A: Following hyperpolarization to −80 mV, voltage was stepped to values ranging from −100 mV to 0 mV, and then to −30 mV (*bottom*). Current trace examples during the range of voltage steps (*i*) showed the activation characteristics of the outward, slowly inactivating current, whereas current trace examples during the final step to −30 mV (*ii*) showed the inactivation characteristics. B: Representative trace showing the A-current (*i*; arrowhead points to A-current), which largely inactivated prior to the peak of the slower outward current. Addition of 4-AP eliminated the presence of the A-current (*ii*). Asterisks indicate capacitive transients. C: The maximum conductance values in response to depolarizing voltage steps were used to calculate the activation curve, while the maximum conductance values in response to a step to −30 mV were used to measure the inactivation curve (*i*, dashed lines). Conductances were calculated using $g = I/(V - E)$ and an experimentally derived reversal potential (E) of −93.1 mV. The normalized activation and inactivation curves are also shown (*ii*, dashed lines; $V_{1/2a} = -22.5 \pm 1.3$ mV, $k_a = 8.1 \pm 3.6$ mV; $V_{1/2i} = -60.2 \pm 1.0$ mV, $k_i = -5.7 \pm 1.1$ mV). D: Following hyperpolarization (gray) and depolarization (black), subthreshold *I-V* curves (*i*) were only slightly different, and resistance curves (*ii*) were not significantly different, indicating that the pertinent current activated in the suprathreshold voltage range.

such as the AHP depth and duration. Recruitment of the K^+ current following hyperpolarization should change spike parameters so as to decrease membrane excitability. For example, a cumulative loss of Na^+ current or an increase of K^+ current can lead to a divisive change in the *f-I* curve by altering the spike rate of rise or the AHP depth and duration, respectively (Fleidervish et al., 1996; Melnick et al., 2004; Mehaffey, 2005; Higgs et al., 2006; Fernandez and White, 2010).

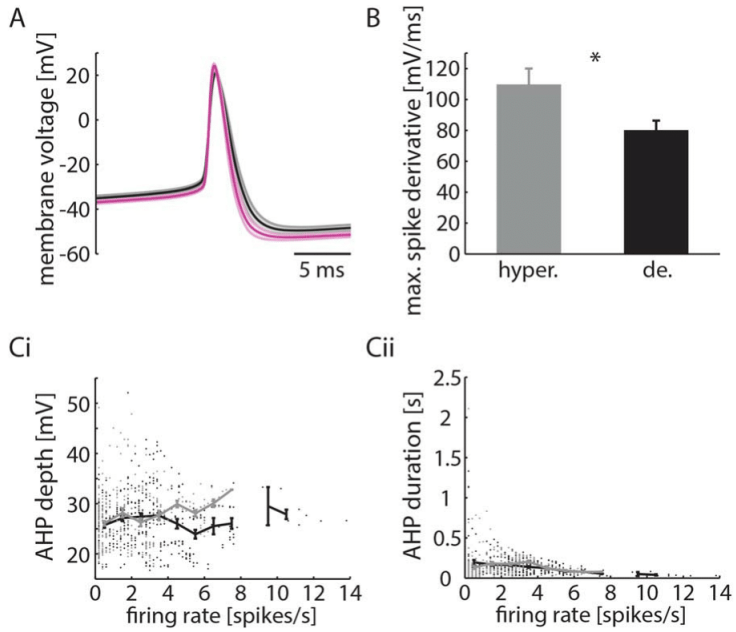

FIGURE 6. Characterization of spike shape following hyperpolarization. A: Average spike shape following hyperpolarization (purple) and depolarization (black). B: Average maximum derivative of the spikes used for A. Spikes following hyperpolarization had a significantly faster rise time, consistent with greater Na^+ conductance availability during the rising phase of the spike. C: AHP depth (*i*) following hyperpolarization (gray) was unaffected for low frequencies (0.2 − 4 Hz), although significantly deeper AHPs were seen at higher frequencies (4.2 − 7 Hz) than those seen following depolarization (black). AHP duration (*ii*) did not change following hyperpolarization. [Color figure can be viewed at wileyonlinelibrary.com]

To make these measures and test if recruitment of the K^+ current following hyperpolarization could alter spike shape, we took the average membrane voltage of spikes following hyperpolarization and compared it to the average spike generated following depolarization. To maximize the potential for observing differences in spike shape, we took the average spike waveform from the last spike of the current step that generated the highest mean firing rate (4.4 ± 0.5 spikes/s); higher firing rates have been established to generate greater spike frequency adaptation and alterations in spike waveform (Fleidervish et al., 1996; Fernandez and White, 2010). Thus, if there were four spikes following hyperpolarization, then the fourth spike was also selected from the corresponding current step following depolarization (Fig. 6A; $n = 24$ neurons).

To start, we measured the rate of rise, a surrogate for Na^+ current availability. Although an unlikely candidate for the observed decrease in gain, we nevertheless measured Na^+ current availability to eliminate the possible explanation of Na^+ current loss through a more complex interaction with K^+ currents and membrane voltage. Furthermore, past work has shown that a loss of Na^+ current can significantly impact gain (Fernandez and White, 2010). As indicated by the maximum derivative of the spike, we observed a steeper rate of rise in the spike waveform, and hence greater availability of Na^+ current, following hyperpolarizing pulses, a result inconsistent with reduced membrane excitability, firing rate, and gain (109.5 ± 10.5 mV/ms following hyperpolarization vs. 79.9 ± 6.4 mV/ms following depolarization; Fig. 6B; $P < 0.001$, two-tailed paired *t*-test; $n = 24$ neurons). Instead, our results are consistent with conventional explanations for increases in firing rate following hyperpolarization: hyperpolarization deinactivates Na^+ channels, allowing greater activation of those channels during subsequent depolarizing inputs. Thus, despite an increase in Na^+ current availability, hyperpolarization still led to a substantial decrease in the excitability of cholinergic neurons. An increase in the depth and duration of the AHP could indicate an increase in K^+ current availability that could account for the reduction in gain (Mehaffey, 2005; Higgs et al., 2006) following hyperpolarization. We characterized the AHP by measuring its depth and duration (see Methods) at various frequencies (1 spike/s sized frequency bins). We observed a slight, non-significant increase in AHP depth following hyperpolarization (Fig. 6Ci; $P = 0.0799$, two-way ANOVA; $n = 35$ neurons). The AHPs at higher frequencies (4.2 to 7 spikes/s) had a significantly different average depth (29.1 ± 0.4 mV following hyperpolarization vs. 24.9 ± 0.6 mV following depolarization; $0.0006 \leq P \leq 0.0495$; two-tailed unpaired *t*-tests for each frequency bin; $n = 3$ to 10 neurons).

This is in contrast to firing rates at or below 4 spikes/s, in which AHP depths were not significantly different (26.8 ± 0.2 mV following hyperpolarization vs. 27.0 ± 0.2 mV following depolarization; $0.3 \leq P \leq 0.6$; two-tailed unpaired *t*-tests for each frequency bin; $n = 8$ to 35 neurons). AHP durations also remained unchanged between the two conditions, with average durations of 151.3 ± 6.0 ms following hyperpolarization and 148.8 ± 5.0 ms following depolarization (Fig. 6Cii; $P = 0.6773$, two-way ANOVA; $n = 35$ neurons).

In summary, although we observed an increase in AHP depth at higher frequencies following hyperpolarization, changes to spike shape were very modest relative to the changes in firing rate and gain. In particular, compared to previous studies linking spike shape and gain (Kernell, 1965; Baldissera and Gustafsson, 1974; Madison and Nicoll, 1984), the changes we observed in cholinergic neurons were small and seem unlikely to influence gain. This is consistent with the slow kinetics of the K^+ current, which significantly limit recruitment within the time frame of an individual spike.

The Introduction of a Slowly Inactivating, Outward K^+ Current Allows for a Subtractive, but not Divisive, Change in the *f-I* Curve of a Model Neuron with a Steep *f-V* Curve

Although the recruitment of the K^+ current did not significantly influence spike shape, we speculated that it could significantly alter gain through another mechanism. To further explore the issue, we used the voltage-clamp data of the K^+ current in conjunction with a spike generating model to probe how or if a slow K^+ current could be recruited during spiking and influence threshold and gain.

For our model, we chose the exponential leaky integrate-and-fire (eLIF) model; this model is effective at reproducing a wide range of electrophysiological behaviors with a relatively small number of parameters (Fourcaud-Trocmé et al., 2003; Brette and Gerstner, 2005; Clopath et al., 2007; Naud et al., 2008; Fernandez et al., 2015). Critically, unlike the standard leaky integrate-and-fire (LIF) model, this model incorporates a real spike threshold. For the passive membrane properties used in the eLIF, we used values for input resistance and capacitance from the range of values we observed experimentally ($R = 118$-760 MΩ; $C = 39$-163 pF). Where possible, all model parameters matched the mean measured values from our experiments (see Methods). In accordance with previous studies that have used the eLIF model, we chose a value of $\Delta_T = 2$ mV (Δ_T: 1-6 mV, Fourcaud-Trocmé et al., 2003; 2 mV, Brette and Gerstner, 2005; 3.48 mV, Geisler et al., 2005; 0.8-5.5 mV, Naud et al., 2008; 2 mV, Touboul and Brette, 2008; 3.4-6.5 mV, Platkiewicz and Brette, 2010; 3 mV, Steimer and Schindler, 2015). Finally, we introduced the slowly inactivating K^+ current (I_{siK}) observed in our voltage-clamp data, with a reversal of -93.1 mV and a maximum conductance of 30.1 nS. Noise was also added to the model (SD = 0.6 ± 0.0006 mV) to mimic the relatively large intrinsic membrane voltage fluctuations present in these neurons in the presence of synaptic blockers (SD = 0.6 ± 0.1 mV at -81.5 ± 0.2 mV) (White et al., 2000).

To measure the *f-I* curve in the model neuron, we delivered a 200 pA range of current in 5 pA steps, with steps following either hyperpolarization (-79.5 ± 0.0009 mV) or depolarization (-58.0 ± 0.0006 mV), similar to our *in vitro* experimental protocol.

As shown, hyperpolarization has a largely subtractive effect on the *f-I* curve, with a gain of 734.0 ± 0.9 spikes/nA·s following hyperpolarization and 557.5 ± 16.3 spikes/nA·s following depolarization that results in a change in normalized gain $\left(\frac{\text{hyperpolarized}}{\text{depolarized}}\right)$ of 1.3 ± 0.04 (Fig. 7B, inset; $n = 50$ simulations). In this case, the lower gain following depolarization is due to the influence of small amounts of noise-induced spikes at low currents on the average *f-I* and *f-V* curve slopes; the current step-induced spiking increased with a slope very similar to hyperpolarized simulations. To better understand why hyperpolarization did not reduce the gain of the *f-I* curve, we plotted the relationship between firing rate and I_{siK}. Although hyperpolarization leads to an initial increase in I_{siK} relative to the depolarized condition, the difference in I_{siK} recruitment remains constant with increasing firing rates (Fig. 7C). Because of the voltage-dependent nature of I_{siK}, we next plotted the *f-V* curve to see if increasing firing rate in the model is associated with depolarization. The model expresses a steep *f-V* curve, with a gain of 84.8 ± 3.8 spikes/mV·s following hyperpolarization and 22.4 ± 4.6 spikes/mV·s following depolarization. Thus membrane voltage is effectively clamped to a near-threshold voltage that precludes significant activation of I_{siK} (Fig. 7D). In other words, the small range of voltages (0.6 ± 0.03 mV; from -58.2 ± 0.03 mV to -57.6 ± 0.004 mV for pulses following hyperpolarization) over which spikes are generated prevents increases in firing rate from recruiting greater amounts of I_{siK}. For this reason, hyperpolarization leads to a translation of the frequency vs. I_{siK} activation curve. On the other hand, a divisive effect on the *f-I* curve would be associated with a frequency-dependent recruitment of the current, with increasing depolarization generating greater activation of I_{siK}.

Cholinergic MS-DB Neurons Have Shallow *f-V* Curves

Our modeling results suggest that a steep *f-V* curve prevents a slowly activating and voltage-dependent K^+ current from increasing its activation level with increasing firing rate. However, the nature of the *f-V* curve in cholinergic MS-DB neurons in unknown. Our previous work in medial entorhinal cortical stellate neurons has shown that neurons can express shallow *f-V* curves that significantly depart from those expressed in established models of spike discharge (Fernandez et al., 2015).

We measured the *f-V* curves by averaging the membrane potential during each current pulse used for the *f-I* curves. We also measured the firing rate using the same methods as the *f-I* curves. In contrast to our model, we found an extremely shallow *f-V* curve that overlapped substantially with the slow K^+ conductance activation curve. Similar to the experimental *f-I* curves, trials where current pulses followed hyperpolarization

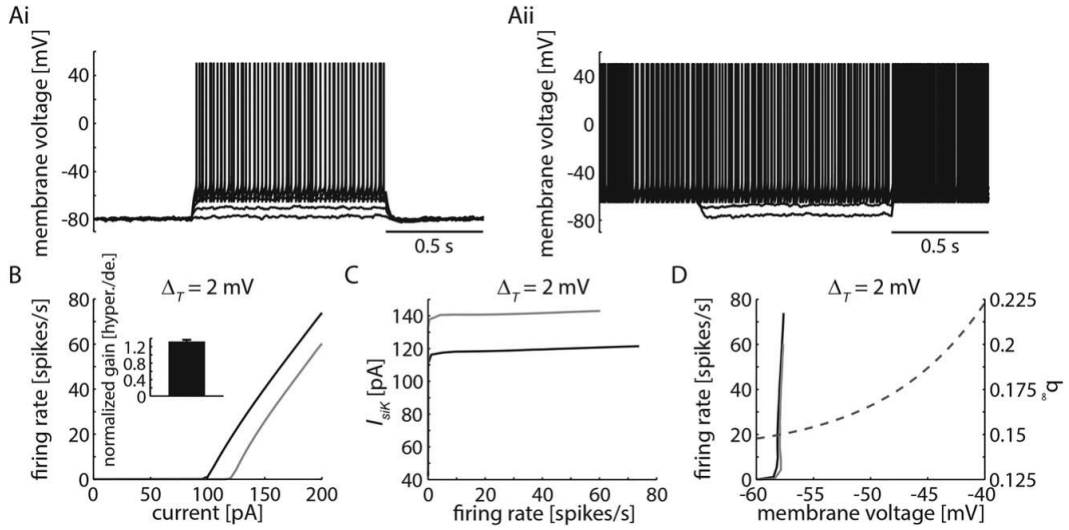

FIGURE 7. eLIF model ($\Delta_T = 2$ mV) with a slowly inactivating K^+ current (I_{siK}) and steep *f-V* curve shows a subtractive change in the *f-I* curve. A: Example traces from the model show similar spiking characteristics following hyperpolarization (*i*) and depolarization (*ii*). B: Model shows a subtractive, rather than divisive, *f-I* curve change following hyperpolarization. C: I_{siK} levels are steady across a range of firing rates, and the difference in current following hyperpolarization and depolarization remains constant. D: Model *f-V* curves are similar following hyperpolarization and depolarization; both are steep and effectively clamp voltage to a narrow range, despite the wide range of firing rates, preventing an increase in I_{siK} activation (dashed line).

resulted in a shallower *f-V* curve than those following depolarization. The gains in these instances were significantly different at 0.1 ± 0.1 spikes/mV·s following hyperpolarization and 0.2 ± 0.1 spikes/mV·s following depolarization (Fig. 8B, inset; $P = 0.042$, two-tailed paired *t*-test; $n = 31$ neurons).

Firing occurred over a wide range of 6.5 ± 0.8 mV (-48.5 ± 1.0 mV to -43.7 ± 0.8 mV; Fig. 8B; $n = 23$ neurons) following hyperpolarization and 7.6 ± 1.1 mV (-47.0 ± 0.9 mV to -40.3 ± 1.1 mV; Fig. 8B; $n = 29$ neurons) following depolarization. Similarly, the average suprathreshold interspike voltage had a range of 6.8 ± 0.8 mV (-47.2 ± 0.8 mV to -40.3 ± 0.7 mV) following hyperpolarization and 9.0 ± 1.2 mV (-45.6 ± 0.7 mV to -36.5 ± 1.1 mV) following depolarization, confirming the large changes in voltage with increases in injected current and firing rate (Fig. 8C). The shallow *f-V* curve in cholinergic MS-DB neurons is in contrast to the steep *f-V* curve of our model neuron and, in agreement with the results from Patel and Burdakov (2015), provides a means whereby the slowly inactivating and voltage-dependent K^+ current can increase its activation as a function of spike firing rate.

Gain Changes through the Introduction of a Slowly Inactivating K^+ Current Require Shallow *f-V* Curves in an eLIF Model

We hypothesized that the voltage-dependent nature of the slowly inactivating K^+ current, combined with the shallow *f-V* curves we observed in cholinergic MS-DB neurons, allow for the current to be recruited in a spike frequency-dependent manner and decrease the *f-I* curve gain. In order to confirm our hypothesis, we changed our model to include a shallow *f-V* curve. Because our previous work has shown that the Δ_T variable in the eLIF model has a drastic effect on the slope of the *f-V* curve (Fernandez et al., 2015), we chose a larger $\Delta_T = 10$ mV in order to obtain a shallower *f-V* curve.

We found that increasing Δ_T to 10 mV results in a 0.5 ± 0.02-fold reduction in gain, with gains of 79.0 ± 2.7 spikes/nA·s following hyperpolarization (-79.1 ± 0.001 mV) and 170.3 ± 7.0 spikes/nA·s following depolarization (-46.9 ± 0.001 mV), and hence similar to the 0.5-fold change seen in our experiments (Fig. 9B, inset; $n = 50$ simulations). The reduction in gain holds true for a range of $V_{1/2}$ values (normalized gains of 0.81 ± 0.04 to 0.08 ± 0.003 following hyperpolarization for {$V_{1/2}$ activation, $V_{1/2}$ inactivation} = {-21.46, −59.23} mV to {-32.46, −70.23} mV, respectively) and *k* values (normalized gains of 0.92 ± 0.04 to 0.16 ± 0.01 following hyperpolarization for {*k* activation, *k* inactivation} = {13.08, −0.69} mV to {6.08, −7.69} mV, respectively), indicating that a reduction in gain could be attained with a range of parameters. In contrast to our results with $\Delta_T = 2$ mV, I_{siK} activation increases with increasing spike firing rate once $\Delta_T = 10$ mV and the *f-V* curve is shallow. Following hyperpolarization, more I_{siK} was recruited per spike, as well as on average at maximum firing rates compared to values following depolarization (Fig. 9C). The *f-V* curve of the model with $\Delta_T = 10$ mV is shallow, with a gain of 0.4 ± 0.02 spikes/mV·s following hyperpolarization and 3.0 ± 0.3 spikes/

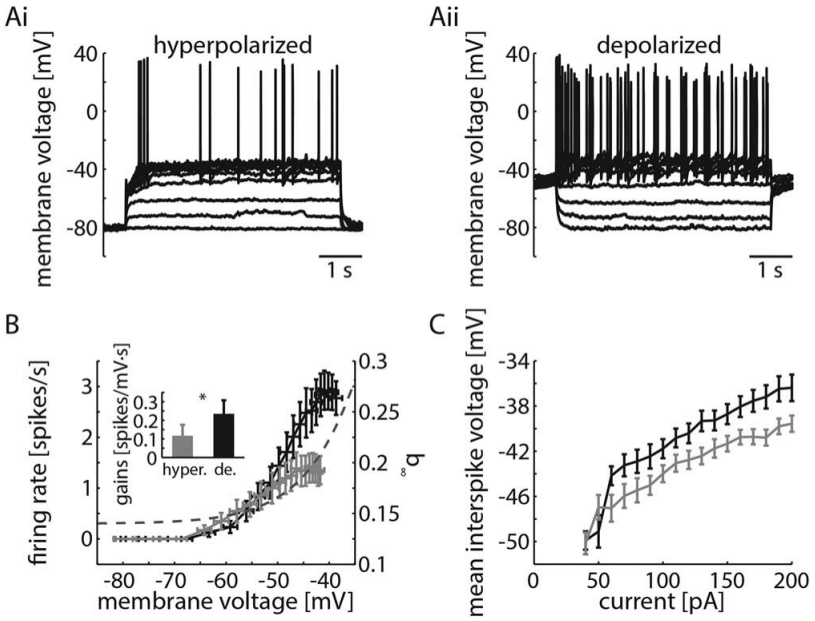

FIGURE 8. Cholinergic neurons in the MS-DB had shallow *f-V* curves. A: Example voltage traces from a cholinergic MS-DB neuron following hyperpolarization (*i*) and depolarization (*ii*). B: These neurons had shallow *f-V* curves which overlapped with the slow K^+ current activation (dashed line) to a greater degree than the model and were divisively changed following hyperpolarization. C: Suprathreshold *I-V* curves following hyperpolarization and depolarization spanned a wide range of voltages, which is consistent with the shallow *f-V* curves.

mV·s following depolarization; spiking occurred over a wide range of voltages (5.1 ± 0.1 mV; from -49.3 ± 0.1 mV to -44.2 ± 0.1 mV for pulses following hyperpolarization), with more overlap with the range of voltages over which the slow K^+ current activated (Fig. 9D).

A shallow *f-V* curve is a critical feature for *f-I* gain changes in our model. Consistent with the results from Patel and Burdakov (2015), we have shown with our modeling and experimental work that gain changes by I_{siK} are possible when the voltage window (the voltage range shown in the *f-V* and suprathreshold *I-V* curves in Figs. 8B and 8C, respectively) overlaps with the activation curve of the current (Fig. 5Cii). This is more likely with a wide voltage window, or when the *f-V* curve is shallow. Thus, our model shows that divisive changes to the *f-I* curve are possible with introduction of a slowly inactivating, outward K^+ current, provided the neuron also has an *f-V* curve with a shallow profile. Hyperpolarization acts to allow recruitment of the K^+ current, reducing both the firing rate and gain.

DISCUSSION

We present evidence of changes in the input-output properties of cholinergic MS-DB neurons in response to hyperpolarizing inputs. These changes, which include reductions in firing rate and gain, are specific to cholinergic neurons. Further, we measured and characterized a slowly inactivating K^+ current and an experimentally verified shallow *f-V* curve, which together can account for the reduction in gain following hyperpolarization.

Implications for Cholinergic MS-DB Neuron Control of Hippocampal Theta Oscillations

Cholinergic MS-DB neurons receive local input from GABAergic and glutamatergic neurons, as well as excitatory input from the hypothalamus and inhibitory feedback from hippocamposeptal neurons (Gerashchenko et al., 2001; Colom et al., 2005; Leão et al., 2015). Since their relay of depolarizing inputs to hippocampal pyramidal and basket neurons may control the amplitude of hippocampal theta, modulation of cholinergic MS-DB neuron gain may change the hippocampal oscillatory state.

Our present work suggests that hyperpolarization acts as a switch by which cholinergic MS-DB neuron spike firing rate and gain is controlled. When cholinergic MS-DB neuron gain is high (without hyperpolarization), their responsiveness to synaptic input is high, which likely increases the amount of acetylcholine delivered to hippocampal neurons. Cholinergic input

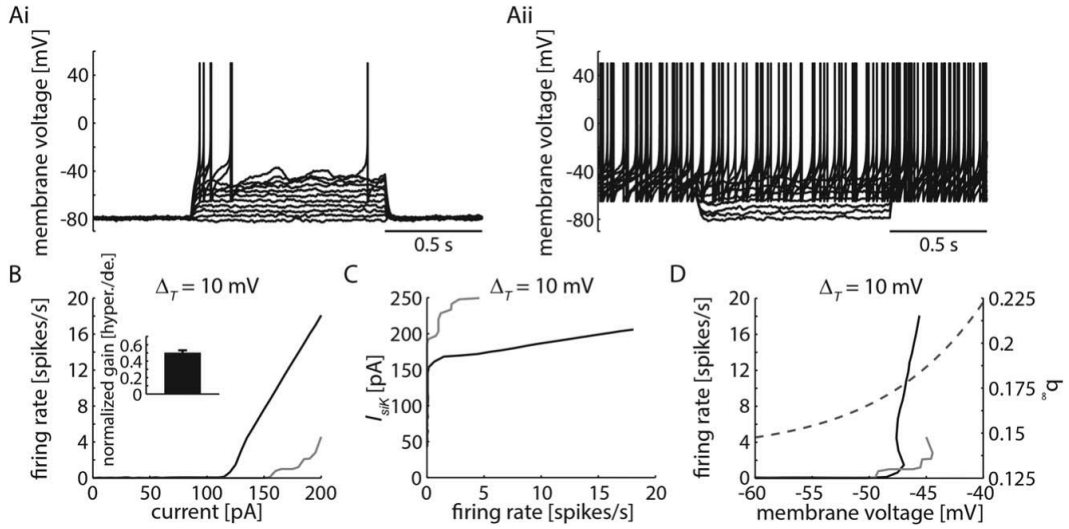

FIGURE 9. eLIF model ($\Delta_T = 10$ mV) with I_{siK} and a shallow *f-V* curve shows a divisive change in the *f-I* curve. A: Example traces from the model show much lower firing rates following hyperpolarization (*i*) than those following depolarization (*ii*). B: Model shows a divisive *f-I* curve change, with a normalized change in gain that is similar to experimental results (*inset*), following hyperpolarization. C: I_{siK} levels change across a range of firing rates, with steeper increases and higher maximum current values evoked following hyperpolarization. D: Model *f-V* curves with $\Delta_T = 10$ mV are shallow following hyperpolarization, covering a range of voltages that increases I_{siK} activation (dashed line) as firing rate increases.

to the hippocampus is responsible for long-lasting depolarization of hippocampal neurons (Dodd et al., 1981; Cole and Nicoll, 1983, 1984), possibly promoting theta. On the other hand, when cholinergic MS-DB neuron gain is low (following hyperpolarization), their responsiveness to synaptic input will also be low, decreasing the amount of acetylcholine released on hippocampal neurons, and thus decreasing theta amplitude. In addition, cholinergic MS-DB neurons may also be indirectly involved in hippocampal theta via their local connections to GABAergic and glutamatergic neurons.

Implications for Cholinergic MS-DB Neuron Control of Hippocampal SPW-Rs

Previous work has shown that MS-DB neuronal activity is suppressed during SPW-R events (Dragoi et al., 1999). Mattis et al. (2014) reported that optogenetic stimulation of hippocamposeptal inhibitory neurons at SPW-R frequencies (50 Hz) was more effective at driving long-lasting hyperpolarization of cholinergic MS-DB neurons than theta frequency stimulation (8 Hz). When taken together with our results, this suggests that SPW-R frequencies in the hippocampus actively suppress theta rhythms though hyperpolarization of cholinergic MS-DB neurons. This hyperpolarization, in turn, may lower the gain of cholinergic MS-DB neurons and decrease their contribution to the hippocampal theta rhythm. On the other hand, when hippocamposeptal neurons (which reflect hippocampal pyramidal neuron firing rates) fire at theta frequencies, cholinergic MS-DB neurons are not as hyperpolarized, their gain is not suppressed, and they can respond with greater sensitivity to local and non-local inputs.

One caveat to this hypothesis is that single SPW-R events are of shorter duration than the SPW-R frequency stimulation of hippocamposeptal neurons performed in Mattis et al. (2014), and thus may not lead to large hyperpolarization of cholinergic neurons. However, it is possible that shorter duration SPW-R frequency hippocamposeptal neuron activity still has significant effects on cholinergic neuron membrane voltage and gain. Also consistent with this hypothesis, a recent study has shown that optogenetic activation of cholinergic MS-DB neurons blocked SPW-Rs in the hippocampus, while increasing theta power and coherence (Vandecasteele et al., 2014). It is therefore possible that hippocamposeptal neurons *dis*inhibit SPW-Rs by suppressing cholinergic MS-DB neuronal activity.

The degree of hyperpolarization presented in Figure 1 is larger than that seen in Mattis et al. (2014), and thus the resulting effect may be larger than under more physiological conditions. Our analysis of the levels of hyperpolarization necessary to evoke the effect, however, suggests that the reduction in firing rate comes on gradually as hyperpolarization increases, such that even small levels of hyperpolarization result in some level of firing rate reduction. In addition, membrane potential in other types of neurons in awake and anesthetized mice is dominated by large (SD $>$ 2 mV), low frequency ($f <$ 5 Hz)

fluctuations (Paré et al., 1998; Destexhe et al., 2003; Crochet and Petersen, 2006; Constantinople and Bruno, 2011; Sachidhanandam et al., 2013). If present in cholinergic MS-DB neurons *in vivo*, low frequency membrane potential fluctuations could elicit robust changes in gain. Moreover, the gain reduction persisted in the presence of artificially-generated membrane voltage fluctuations mimicking *in vivo* conditions. It would be possible to test the effects of hippocamposeptal-induced hyperpolarization by testing the gain of cholinergic MS-DB neurons following optogenetic stimulation of hippocamposeptal axons or neurons.

Future *in vivo* experiments that test the role of hyperpolarization-induced gain reduction in the disinhibition of SPW-Rs will be needed. If our hypothesis is correct, selective block of the slowly inactivating K^+ current present in cholinergic MS-DB neurons may lead to learning deficits due to impaired SPW-Rs and memory consolidation. In addition, Mattis et al. (2014) reported that long-lasting hippocamposeptal hyperpolarization of cholinergic neurons was sensitive to GIRK channel and D_2 dopamine receptor antagonists. This G-protein-coupled response is in contrast to the GABAergic response evoked by theta frequency stimulation of hippocamposeptal neurons. Therefore, it may be possible to observe reductions in the firing rate and gain of these neurons, and perhaps increases in hippocampal SPW-Rs, through local application of GIRK channel and D_2 receptor agonists.

Voltage-Dependent Gain Modulation in Cholinergic MS-DB Neurons

Our voltage-clamp measures indicate the presence of a slowly activating and inactivating K^+ current that activates at suprathreshold voltage values. In combination with the shallow *f-V* curve, the increased activation of the K^+ current leads to a divisive effect on the *f-I* curve of cholinergic neurons. The divisive change occurs when depolarization increases with firing rate (shallow *f-V* curve), which enables the K^+ current to increase its average conductance at higher spike firing rates.

Generally, models of spike discharge express a flat *I-V* curve, along with a correspondingly steep *f-V* curve (Holt and Koch, 1997; Mitchell and Silver, 2003; Prescott and De Koninck, 2003). In fact, a flat *I-V* curve is a feature that has been used to account for the numerous effects of synaptic input and shunting conductance on input-output modulation in neurons (Holt and Koch, 1997; Doiron et al., 2001; Ulrich, 2003). In particular, Holt and Koch (1997) describe an LIF model in which the spiking mechanism clamps membrane voltage to approximately −50 mV. Because the voltage trajectory between spikes in the LIF model is exponential, with a relatively short membrane time constant, membrane voltage largely hovers near the asymptotic value. This, along with the spike reset mechanism, effectively clamps membrane voltage during spiking somewhere between the reset value and the asymptotic value of the exponential trajectory. Further, increasing the spike firing rate does little to change the mean voltage trajectory since the mean of an individual exponential trajectory between spikes changes little with higher input currents.

Positively sloped and shallow *f-V* curves, however, may be a common characteristic of biological neurons (Fernandez et al., 2011, 2015; our present work). In part, this is because the evolution of the membrane voltage trajectory between spikes is rarely exponential, as it is influenced by numerous voltage-gated conductances that activate, deactivate or inactivate during and after the spike refractory period. As a result, in biological neurons, the mean value of the voltage trajectory during spiking can depolarize with increasing firing rate and input current. This is in sharp contrast to the linear behavior in the LIF that can only generate an exponential trajectory, whereby the firing rate has little impact on the mean voltage value during spiking.

It is common for studies using the eLIF model to use small Δ_T values, as it accurately reproduces the spike onset behavior observed in biological neurons. Under these conditions, however, the *f-V* curve remains similar to the LIF model. This is because the evolution of the membrane voltage trajectory is largely exponential and is only influenced by the Δ_T parameter in the immediate vicinity of spike threshold. The shallow *f-V* curve we measured in cholinergic MS-DB neurons led us to choose a Δ_T value of 10 mV that generates a shallow *f-V* curve in accordance to mechanisms described by Fernandez et al. (2015). Although $\Delta_T = 10$ mV is higher than Δ_T values derived from analysis of neuronal Na^+ channel activation kinetics (Angelino and Brenner, 2007), it provides a simple method by which to reproduce a fundamental feature of neuronal *f-V* curves. The origin of shallow *f-V* curves is complex and likely originates from a multitude of factors that differ between neuron types, and are beyond the scope of this paper. Fundamentally, the expression of a shallow *f-V* curve is critical, as neurons express voltage-gated conductances with similarly shallow activation curves. Thus, whether our simplified model accurately describes the biophysical origin of the shallow *f-V* curve is of secondary importance to the fact that it generates a more biologically accurate *f-V* relationship. Once present, the model with a shallow *f-V* curve easily scales its firing rate and gain in the presence of a slowly activating and inactivating K^+ conductance.

Identity of the Slowly Inactivating Outward Current

The simplest way to test the role of the slowly inactivating outward current in the input-output properties of cholinergic MS-DB neurons would be to use specific channel antagonists. By using a specific blocker of the current, we would be able to observe if hyperpolarizing inputs still cause subsequent reductions in firing rate and gain. Because of the −93.1 mV reversal potential, indicating a K^+ dominated current, and because of the slow activation and inactivation kinetics of the current, we selected blockers of Kv1, Kv7, and other K^+ channels. Although we attempted to block the current with 4-AP, XE991, hongotoxin-1, and TEA, none of the drugs completely and specifically blocked the current. TEA did block the current, but in

a non-specific way, making it impossible to ascertain the influence of the current on input-output properties. Future work will be needed to identify the constituent channels of the current, providing a means whereby their necessity in firing rate and gain reductions can be tested more directly.

REFERENCES

Alonso A, Köhler C. 1982. Evidence for separate projections of hippocampal pyramidal and non-pyramidal neurons to different parts of the septum in the rat brain. Neurosci Lett 31:209–214.

Anderson JS, Lampl I, Gillespie DC, Ferster D. 2000. The contribution of noise to contrast invariance of orientation tuning in cat visual cortex. Science 290:1968–1972.

Angelino E, Brenner MP. 2007. Excitability constraints on voltage-gated sodium channels. PLoS Comput Biol 3:1751–1760.

Baldissera F, Gustafsson B. 1974. Firing behaviour of a neurone model based on the afterhyperpolarization conductance time course and algebraical summation. Adaptation and steady state firing. Acta Physiol Scand 92:27–47.

Bekkers JM. 2000. Properties of voltage-gated potassium currents in nucleated patches from large layer 5 cortical pyramidal neurons of the rat. J Physiol 525:593–609.

Berry SD, Thompson RF. 1978. Prediction of learning rate from the hippocampal electroencephalogram. Science 200:1298–1300.

Brette R, Gerstner W. 2005. Adaptive exponential integrate-and-fire model as an effective description of neuronal activity. J Neurophysiol 94:3637–3642.

Buzsáki G. 2005. Theta rhythm of navigation: link between path integration and landmark navigation, episodic and semantic memory. Hippocampus 15:827–840.

Chapman CA, Lacaille J-C. 1999. Cholinergic induction of theta-frequency oscillations in hippocampal inhibitory interneurons and pacing of pyramidal cell firing. J Neurosci 19:8637–8645.

Clopath C, Jolivet R, Rauch A, Lüscher H-R, Gerstner W. 2007. Predicting neuronal activity with simple models of the threshold type: adaptive exponential integrate-and-fire model with two compartments. Neurocomputing 70:1668–1673.

Cole AE, Nicoll RA. 1983. Acetylcholine mediates a slow synaptic potential in hippocampal pyramidal cells. Science 221:1299–1301.

Cole AE, Nicoll RA. 1984. Characterization of a slow cholinergic post-synaptic potential recorded in vitro from rat hippocampal pyramidal cells. J Physiol 352:173–188.

Colom LV, Castaneda MT, Reyna T, Hernandez S, Garrido-Sanabria E. 2005. Characterization of medial septal glutamatergic neurons and their projection to the hippocampus. Synapse 58:151–164.

Connor JA, Stevens CF. 1971. Prediction of repetitive firing behaviour from voltage clamp data on an isolated neurone soma. J Physiol 213:31–53.

Constantinople CM, Bruno RM. 2011. Effects and mechanisms of wakefulness on local cortical networks. Neuron 69:1061–1068.

Crochet S, Petersen CCH. 2006. Correlating whisker behavior with membrane potential in barrel cortex of awake mice. Nat Neurosci 9:608–610.

Destexhe A, Rudolph M, Paré D. 2003. The high-conductance state of neocortical neurons in vivo. Nat Rev Neurosci 4:739–751.

Dodd J, Dingledine R, Kelly JS. 1981. The excitatory action of acetylcholine on hippocampal neurones of the guinea pig and rat maintained in vitro. Brain Res 207:109–127.

Doiron B, Longtin A, Berman N, Maler L. 2001. Subtractive and divisive inhibition: Effect of voltage-dependent inhibitory conductances and noise. Neural Comput 13:227–248.

Dragoi G, Carpi D, Recce M, Csicsvari J, Buzsáki G. 1999. Interactions between hippocampus and medial septum during sharp waves and theta oscillation in the behaving rat. J Neurosci 19:6191–6199.

Fernandez FR, Broicher T, Truong A, White JA. 2011. Membrane voltage fluctuations reduce spike frequency adaptation and preserve output gain in CA1 pyramidal neurons in a high-conductance state. J Neurosci 31:3880–3893.

Fernandez FR, Malerba P, White JA. 2015. Non-linear membrane properties in entorhinal cortical stellate cells reduce modulation of input-output responses by voltage fluctuations. PLoS Comput Biol 11:e1004188.

Fernandez FR, White JA. 2010. Gain control in CA1 pyramidal cells using changes in somatic conductance. J Neurosci 30:230–241.

Fleidervish IA, Friedman A, Gutnick MJ. 1996. Slow inactivation of Na^+ current and slow cumulative spike adaptation in mouse and guinea-pig neocortical neurones in slices. J Physiol 493:83–97.

Fourcaud-Trocmé N, Hansel D, Vreeswijk CV, Brunel N. 2003. How spike generation mechanisms determine the neuronal response to fluctuating inputs. J Neurosci 23:11628–11640.

Geisler C, Brunel N, Wang X-J. 2005. Contributions of intrinsic membrane dynamics to fast network oscillations with irregular neuronal discharges. J Neurophysiol 94:4344–4361.

Gerashchenko D, Salin-Pascual R, Shiromani PJ. 2001. Effects of hypocretin-saporin injections into the medial septum on sleep and hippocampal theta. Brain Res 913:106–115.

Girardeau G, Benchenane K, Wiener SI, Buzsáki G, Zugaro MB. 2009. Selective suppression of hippocampal ripples impairs spatial memory. Nat Neurosci 12:1222–1223.

Griffith WH, Sim JA. 1990. Comparison of 4-aminopyridine and tetrahydroaminoacridine on basal forebrain neurons. J Pharmacol Exp Ther 255:986–993.

Hasselmo ME. 2005. What is the function of hippocampal theta rhythm?–Linking behavioral data to phasic properties of field potential and unit recording data. Hippocampus 15:936–949.

Heath NC, Rizwan AP, Engbers JDT, Anderson D, Zamponi GW, Turner RW. 2014. The expression pattern of a Cav3-Kv4 complex differentially regulates spike output in cerebellar granule cells. J Neurosci 34:8800–8812.

Higgs MH, Slee SJ, Spain WJ. 2006. Diversity of gain modulation by noise in neocortical neurons: regulation by the slow afterhyperpolarization conductance. J Neurosci 26:8787–8799.

Holt GR, Koch C. 1997. Shunting inhibition does not have a divisive effect on firing rates. Neural Comput 9:1001–1013.

Jinno S, Klausberger T, Marton LF, Dalezios Y, Roberts JDB, Fuentealba P, Bushong EA, Henze D, Buzsáki G, Somogyi P. 2007. Neuronal diversity in GABAergic long-range projections from the hippocampus. J Neurosci 27:8790–8804.

Kernell D. 1965. The limits of firing frequency in cat lumbosacral motoneurones possessing different time course of afterhyperpolarization. Acta Physiol Scand 65:87–100.

Kramis R, Vanderwolf CH, Bland BH. 1975. Two types of hippocampal rhythmical slow activity in both the rabbit and the rat: Relations to behavior and effects of atropine, diethyl ether, urethane, and pentobarbital. Exp Neurol 49:58–85.

Leão RN, Targino ZH, Colom LV, Fisahn A. 2015. Interconnection and synchronization of neuronal populations in the mouse medial septum/diagonal band of Broca. J Neurophysiol 113:971–980.

Lee MG, Chrobak JJ, Sik A, Wiley RG, Buzsáki G. 1994. Hippocampal theta activity following selective lesion of the septal cholinergic system. Neuroscience 62:1033–1047.

Lin RJ, Bettencourt J, White JA, Christini DJ, Butera RJ. 2010. Real-time experiment interface for biological control applications. Conf Proc IEEE Eng Med Biol Soc 1:4160–4163.

Madison DV, Nicoll RA. 1984. Control of the repetitive discharge of rat CA1 pyramidal neurones in vitro. J Physiol 354:319–331.

Magariños-Ascone C, Núñez Á, Delgado-García JM. 1999. Different discharge properties of rat facial nucleus motoneurons. Neuroscience 94:879–886.

Markram H, Segal M. 1990. Electrophysiological characteristics of cholinergic and non-cholinergic neurons in the rat medial septum-diagonal band complex. Brain Res 513:171–174.

Mattis J, Brill J, Evans S, Lerner TN, Davidson TJ, Hyun M, Ramakrishnan C, Deisseroth K, Huguenard JR. 2014. Frequency-dependent, cell type-divergent signaling in the hippocamposeptal projection. J Neurosci 34:11769–11780.

Mehaffey WH. 2005. Deterministic multiplicative gain control with active dendrites. J Neurosci 25:9968–9977.

Melnick IV, Santos SFA, Safronov BV. 2004. Mechanism of spike frequency adaptation in substantia gelatinosa neurones of rat. J Physiol 559:383–395.

Mitchell SJ, Silver RA. 2003. Shunting inhibition modulates neuronal gain during synaptic excitation. Neuron 38:433–445.

Naud R, Marcille N, Clopath C, Gerstner W. 2008. Firing patterns in the adaptive exponential integrate-and-fire model. Biol Cybern 99: 335–347.

Paré D, Shink E, Gaudreau H, Destexhe A, Lang EJ. 1998. Impact of spontaneous synaptic activity on the resting properties of cat neocortical pyramidal neurons in vivo. J Neurophysiol 79:1450–1460.

Patel AX, Burdakov D. 2015. Mechanisms of gain control by voltage-gated channels in intrinsically-firing neurons. PLoS One 10: e0115431.

Platkiewicz J, Brette R. 2010. A threshold equation for action potential initiation. PLoS Comput Biol 6:e1000850.

Prescott SA, De Koninck Y. 2003. Gain control of firing rate by shunting inhibition: roles of synaptic noise and dendritic saturation. Proc Natl Acad Sci USA 100:2076–2081.

Sachidhanandam S, Sreenivasan V, Kyriakatos A, Kremer Y, Petersen CCH. 2013. Membrane potential correlates of sensory perception in mouse barrel cortex. Nat Neurosci 16:1671–1677.

Segal M, Barker JL. 1984. Rat hippocampal neurons in culture: potassium conductances. J Neurophysiol 51:1409–1433.

Sotty F, Danik M, Manseau F, Laplante F, Quirion R, Williams S. 2003. Distinct electrophysiological properties of glutamatergic, cholinergic and GABAergic rat septohippocampal neurons: Novel implications for hippocampal rhythmicity. J Physiol 551:927–943.

Steimer A, Schindler K. 2015. Random sampling with interspike-intervals of the exponential integrate and fire neuron: A computational interpretation of UP-states. PLoS One 10:e0132906.

Takács VT, Freund TF, Gulyás AI. 2008. Types and synaptic connections of hippocampal inhibitory neurons reciprocally connected with the medial septum. Eur J Neurosci 28:148–164.

Tóth K, Borhegyi Z, Freund TF. 1993. Postsynaptic targets of GABAergic hippocampal neurons in the medial septum-diagonal band of Broca complex. J Neurosci 13:3712–3724.

Touboul J, Brette R. 2008. Dynamics and bifurcations of the adaptive exponential integrate-and-fire model. Biol Cybern 99:319–334.

Ulrich D. 2003. Differential arithmetic of shunting inhibition for voltage and spike rate in neocortical pyramidal cells. Eur J Neurosci 18:2159–2165.

Vandecasteele M, Varga V, Berényi A, Papp E, Barthó P, Venance L, Freund TF, Buzsáki G. 2014. Optogenetic activation of septal cholinergic neurons suppresses sharp wave ripples and enhances theta oscillations in the hippocampus. Proc Natl Acad Sci USA 111:13535–13540.

White JA, Rubinstein JT, Kay AR. 2000. Channel noise in neurons. Trends Neurosci 23:131–137.

Winson J. 1978. Loss of hippocampal theta rhythm results in spatial memory deficit in the rat. Science 201:160–163.

Zhang H, Lin S-C, Nicolelis MAL. 2011. A distinctive subpopulation of medial septal slow-firing neurons promote hippocampal activation and theta oscillations. J Neurophysiol 106:2749–2763.

Zona C, Pirrone G, Avoli M, Dichter M. 1988. Delayed and fast transient potassium currents in rat neocortical neurons in cell culture. Neurosci Lett 94:285–290.

CHAPTER 3

CHOLINERGIC SUPPRESSION OF HIPPOCAMPAL RIPPLES THROUGH DISRUPTION OF BALANCED EXCITATION/INHIBITION

3.1 Abstract

Sharp wave-ripples (140-220 Hz) are patterns of brain activity, seen in the local field potential of the hippocampus, that are important for memory consolidation. Cholinergic inputs to the hippocampus from neurons in the medial septum-diagonal band of Broca cause a marked reduction in ripple incidence as rodents switch from memory consolidation to memory encoding behaviors. The mechanism for this disruption in ripple power is not fully understood. In isolated neurons, the major effect of cholinergic input on hippocampal neurons is an increase in membrane potential, which affects both hippocampal pyramidal neurons and inhibitory interneurons. Using an existing model of hippocampal ripples that includes both pyramidal neurons and interneurons (Brunel and Wang, 2003), we investigated the mechanism whereby depolarizing inputs to these neurons affects ripple power and frequency. We observed that ripple power and frequency is maintained, as long as inputs to pyramidal neurons and interneurons are balanced. Unequal drive to pyramidal cells or interneurons, however, affects ripple power and can disrupt ripple oscillations by pushing ripple frequency higher or lower, depending on the neuron type being driven harder. Thus, an

imbalance in drive to the pyramidal cells and interneurons required to generate ripples provides a means whereby cholinergic input can suppress hippocampal ripples.

3.2 Introduction

Hippocampal network oscillations are important for learning and memory. Two of these oscillations, theta rhythms (4-12 Hz) and sharp wave-ripple complexes (ripples; 140-220 Hz; O'Keefe, 1976), occur during opposing behaviors. Theta rhythms are involved in attention, navigation, and memory encoding (Berry and Thompson, 1978; Winson, 1978; see Buzsáki, 2005, for review; Hasselmo, 2005), and they occur during exploratory behaviors and REM sleep. On the other hand, ripples are important for memory consolidation (Girardeau et al., 2009; Maingret et al., 2016), and they occur during immobility and slow wave sleep (Buzsáki et al., 1983, 1992).

In the previous chapter, we explored the electrophysiological properties of cholinergic neurons in the medial septum-diagonal band of Broca (MS-DB), which influence both of these rhythms, promoting theta and suppressing ripples (Winson, 1978; Vandecasteele et al., 2014). During ripples, MS-DB neuron firing is suppressed (Dragoi et al., 1999), most likely through feedback connections from the hippocampus (Alonso and Köhler, 1982; Tóth et al., 1993; Jinno et al., 2007; Takács et al., 2008). However, during theta rhythms, acetylcholine (ACh) release from MS-DB neurons increases (Zhang et al., 2010, 2011) and suppresses hippocampal ripples (Vandecasteele et al., 2014). The magnitude of the effects of ACh (or cholinomimetics) on intrinsic properties of hippocampal neurons are relatively well described in the literature (Cole and Nicoll, 1983, 1984; Figenschou et al., 1996; Chapman and Lacaille, 1999;

McQuiston and Madison, 1999a; Tai et al., 2006). Despite knowing the general effects of ACh on individual hippocampal neurons, the mechanisms through which these effects change network dynamics and potentially suppress hippocampal ripples have not been studied.

Using an existing model of hippocampal ripples (Brunel and Wang, 2003), we show that depolarization of hippocampal neurons by ACh may decrease local field potential (LFP) power in the ripple range by disrupting the balance between currents to pyramidal neurons and interneurons, causing different CA1 subnetworks to dominate the LFP. These findings show a possible mechanism for ACh suppression of ripples.

3.3 Materials and Methods

3.3.1 Model architecture

We used a previously published model of hippocampal ripples (see Brunel and Wang, 2003, for detailed methods) as the original model to which we compared the effects of manipulations. This model includes 4000 pyramidal neurons and 1000 interneurons (Fig. 3.1A). All neurons are connected with a probability of 0.2, with the exception of pyramidal-pyramidal connections, which do not exist. The membrane voltage of the leaky integrate-and-fire (LIF) model neurons is governed by the following equation:

$$C\frac{dV}{dt} = -g_L(V - E_L) + I_{AMPA} + I_{NMDA} + I_{GABA} + I_{DC}, \quad (3.1)$$

where C is the membrane capacitance (1 nF), V is the membrane voltage, g_L is the leak conductance (50 nS for pyramidal neurons, 100 nS for interneurons), and E_L is the leak reversal (-70 mV). Thus, pyramidal neurons have a membrane time constant of 20 ms

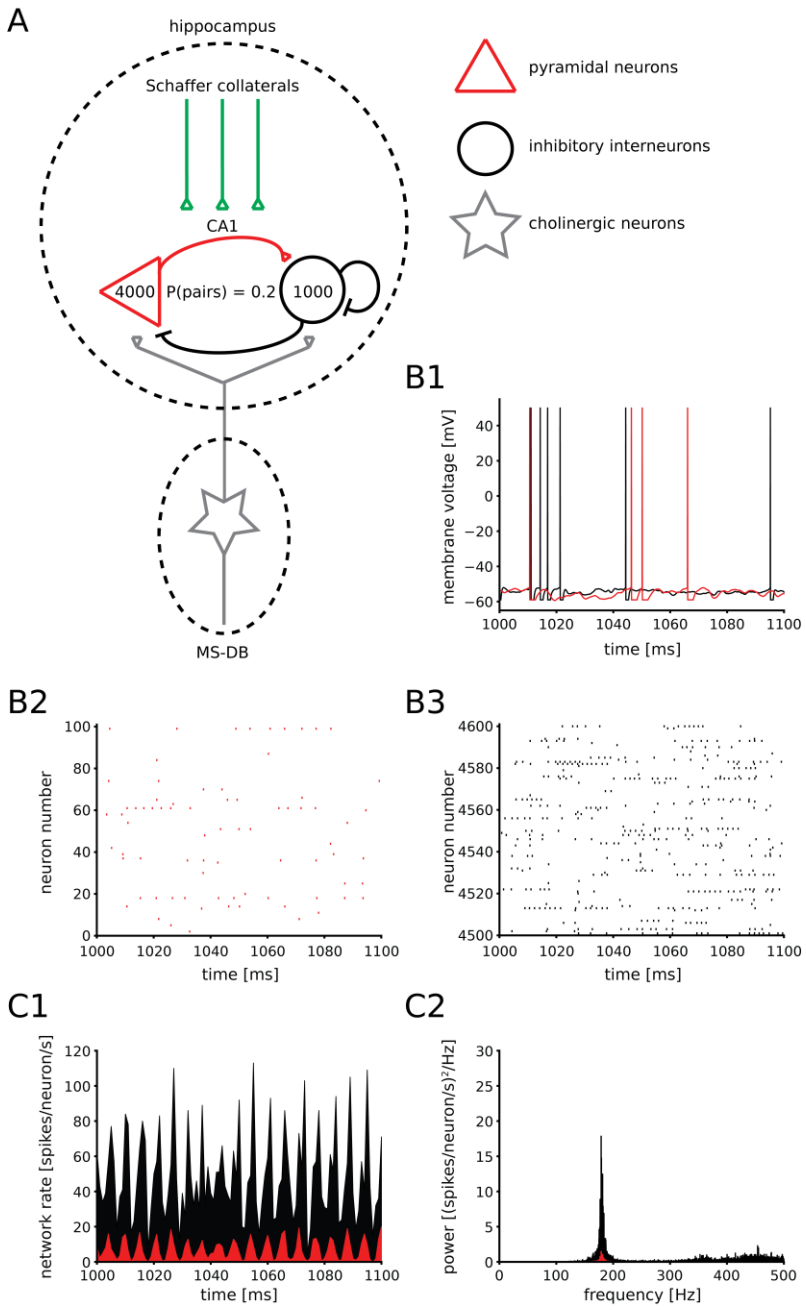

Fig. 3.1. Model of ripples from Brunel and Wang (2003) replicates hippocampal features.

A: Diagram depicting the biophysical model of hippocampal ripples from Brunel and Wang (2003). ***B***: Sample voltage traces from a representative pyramidal neuron (red) and interneuron (black) (***1***). Throughout all figures, red is used to indicate data from pyramidal neurons, and black is used to indicate data from interneurons. Raster plots also show irregular firing in individual pyramidal neurons (***2***) and interneurons (***3***). ***C***: Mean neuron spiking activity across the network, on the other hand, shows a clear oscillation at ripple frequency for both types of neurons (***1***). The power spectra for each neuron type (***2***) shows a strong peak at about 180 Hz.

and interneurons have a time constant of 10 ms. When V exceeds the spike threshold (-52 mV), that simulation time step is set to a spike height of 50 mV, followed by a refractory period (2 ms for pyramidal neurons, 1 ms for interneurons), during which voltage is held at the reset potential (-59 mV).

Synaptic currents (I_{syn}) are governed as follows:

$$I_{syn} = g_{syn}s(t)(V - V_{syn}), \tag{3.2}$$

where g_{syn} is the synaptic conductance, V_{syn} in the synaptic reversal potential (0 mV for AMPA and NMDA, -70 mV for GABA), and $s(t)$ is a function characterizing the synaptic variable, updating after the latency time (τ_l) as follows:

$$s(t) = \frac{\tau_m}{\tau_d - \tau_r}\left[\exp\left(-\frac{t-\tau_l}{\tau_d}\right) - \exp\left(-\frac{t-\tau_l}{\tau_r}\right)\right]. \tag{3.3}$$

In this equation, τ_m is the membrane time constant, τ_l is the latency from a presynaptic spike to the start of a postsynaptic event, τ_r is the rise time constant of synaptic events, and τ_d is the decay time constant of synaptic events. Unless otherwise noted, for simulations in which there were both pyramidal neurons and interneurons, the default synaptic parameters are (in ms) AMPA: $\tau_l = 1$, $\tau_r = 0.4$, $\tau_d = 2$; NMDA: $\tau_l = 1$, $\tau_r = 2$, $\tau_d = 100$; GABA: $\tau_l = 0.5$, $\tau_r = 0.5$, $\tau_d = 5$. For simulations in which there were only interneurons, the default synaptic parameters are (in ms) GABA: $\tau_l = 1$, $\tau_r = 0.5$, $\tau_d = 5$. Values for g_{syn} can be found in Brunel and Wang (2003) and are based on experimental measurements. External drive comes from Schaffer collateral-like AMPA synapses, which have default Poisson rates of 12 kHz for interneuron-only networks and 24 kHz (pyramidal neurons) and 22 kHz (interneurons) for two-population networks. For the pyramidal-interneuron-pyramidal network, the Poisson rates are 24 kHz (pyramidal neurons) and 12 kHz (interneurons).

The model was written in C/C++ and solved using a second-order Runge Kutta algorithm with a time step of 0.05 ms. Simulations were run on the University of Utah's Center for High Performance Computing clusters and lasted approximately 15 minutes.

3.3.2 Data analysis

Data analysis was performed using custom and built-in functions in Python 3.5.2 on the Anaconda 2.4.1 platform (with NumPy, SciPy, Pandas, and Matplotlib libraries). All values and error bars are reported as mean ± SEM. The network rate for each neuron type was the total sum of the spikes from that neuron type during 1 ms bins, divided by the number of neurons of that type. Because of the scarcity of recurrent connections between pyramidal neurons in CA1 and because the ripple LFP is recorded from the pyramidal layer, the interneurons' network rate was used as an LFP surrogate, and all network statistics were measured from this signal. Spike frequency was determined by counting spikes and dividing by time. Power spectra were calculated by taking the FFT of the LFP after the first 500 ms of the simulation in order to allow the network to settle into a steady oscillation. The phase lag of interneurons relative to pyramidal neurons was measured by taking the Hilbert transform of the network rate of each neuron type, and then finding the average difference between the two Hilbert transforms when the phase of pyramidal neurons had a negative to positive zero crossing. Ripple frequency was defined as the peak of the power spectrum in the range [4, 400]. Total ripple power was determined by finding the ripple frequency and taking the integral of the power from 40 Hz below that peak to 40 Hz above it. The ratio of ripple power to low frequency power (or ripple ratio) was then calculated as the total ripple power divided

by the integral of power in the range [4, 50]. The resulting ratio was normalized to the ripple ratio of the baseline simulation (the simulation with no I_{DC} to either neuron type). The normalized ripple ratio is referred to in the paper simply as "ripple ratio".

3.4 Results

To address how cholinergic input suppresses hippocampal ripples, we used an established model of hippocampal ripples (Brunel and Wang, 2003). This model features realistic membrane and synaptic parameters, external drive modeling input from Schaffer collaterals originating in CA3 (Chrobak and Buzsáki, 1996; Csicsvari et al., 2000; Bezaire and Soltesz, 2013), low firing rates of individual neurons (relative to the LFP ripple frequency), and irregular firing patterns that are independent of synchronous population rates (i.e., LFP patterns are not observable except as the sum of the activity of many neurons; see Fig. 3.1B) (Fries et al., 2001; Logothetis et al., 2001). Additionally, the average firing rate of interneurons in the two-population network is ~50 Hz, similar to *in vivo* firing rates of many types of projection neurons during ripples (Jinno et al., 2007). Due to their sparseness (Christian and Dudek, 1988; Thomson and Radpour, 1991), recurrent connections between pyramidal neurons are eliminated from the model, though Brunel and Wang (2003) do consider the effects of pyramidal neurons on ripples in their study. Remaining connection probabilities of the constituent neurons are set at 0.2. This network model establishes a baseline for ripple frequency and power, while the simplified nature of its LIF model neurons gave us the ability to easily manipulate different membrane parameters that change as a result of cholinergic input.

As previously shown, this model produces ripples with a peak frequency at 178.84 Hz (Fig. 3.1C; interneuron total ripple power = 0.4686 (spikes/neuron)^2) (Brunel and Wang, 2003). Owing to the greater number of spikes, and thus downstream synaptic activity, the power spectrum is dominated by the interneurons (Fig. 3.1C2). The network rate of the pyramidal neurons also oscillates at ripple frequencies (pyramidal neuron peak frequency = 178.84 Hz; pyramidal neuron total ripple power = 0.0373 (spikes/neuron)^2). In agreement with data from Maier et al. (2011) and Hulse et al. (2016) showing that inhibition lags behind excitation during ripples, the average phase difference between pyramidal neurons and interneurons is 29.06 ± 1.39 degrees (n = 1793 zero crossings). Thus, this model produces prominent ripple oscillations with realistic relative phase profiles for pyramidal cells and interneurons and provides a baseline with which to compare changes in ripple frequency and power with cholinergic-like depolarization.

3.4.1 Balancing the effects of I_{DC} on steady-state voltage preserves ripples

Cholinergic input has numerous effects on the excitability of individual hippocampal neurons. In pyramidal neurons, muscarinic input increases membrane voltage by approximately 5-14 mV (likely depending on whether iontophoretic ACh application or cholinomimetics were used) (Dodd et al., 1981; Benardo and Prince, 1982; Cole and Nicoll, 1984). Membrane resistance is increased by about 12-19 MΩ (Dodd et al., 1981; Benardo and Prince, 1982; Cole and Nicoll, 1984). The amplitude of the spike afterhyperpolarization (AHP) is decreased (Benardo and Prince, 1982; Cole

and Nicoll, 1984). Spike adaptation is also decreased (Cole and Nicoll, 1984; Madison and Nicoll, 1984). We should note that pyramidal neurons likely have no major nicotinic response (Frazier et al., 1998).

In interneurons, cholinergic effects include an increase in membrane voltage, though the magnitude of this effect varies. Chapman and Lacaille (1999) report an increase of 4.1 ± 0.7 mV in lacunosum-moleculare interneurons, but others report increases as large as 14.5 ± 0.6 mV in interneurons across CA1 layers with only muscarinic input (McQuiston and Madison, 1999a). Changes in membrane resistance depend on interneuron subtype (Chapman and Lacaille, 1999). The effects of nicotinic stimulation on membrane voltage in interneurons also varies, and effects can be categorized into three groups: fast depolarization, fast and slow depolarization, and nonresponsive (McQuiston and Madison, 1999b).

Changes in membrane depolarization, resistance, AHP magnitude, and spike rate adaptation affect spike output and thus may affect ripples. Among these, the depolarizing effects of cholinergic modulation are the most consistent and ubiquitous. The additional effects on resistance, AHP, and spike rate adaptation varied in magnitude, time scale, and neuron type, and were therefore not included in our study. Because of the ubiquity and large magnitude of depolarization among the various types of neurons, we chose to focus on this effect for our model analysis.

We modeled cholinergic depolarization by adding DC current (I_{DC}) to all neurons of either type. Current levels were selected to increase the steady-state membrane voltage of isolated neurons by up to 10 mV (note, model neurons' membrane resistance is constant across voltage and time), which is within the range provided by

cholinergic stimulation. We justify using DC current because the decay time scale of the increase in membrane voltage associated with cholinergic modulation exceeds the length of our simulations (membrane potential increases last for 10s of seconds, much longer than individual ripple events) (Cole and Nicoll, 1984).

As cholinergic modulation occurs in both pyramidal neurons and interneurons, we investigated the effects of combining varying amounts of I_{DC} input to both neuron types. In order to measure relative ripple power across this range of conditions, we measured the ratio of power surrounding the power spectrum peak to power at low frequencies (see Methods).

We found that combining I_{DC} to pyramidal neurons (I_{DCpyr}) and interneurons (I_{DCint}) at a range of values generally drove the network into one of three qualitatively different states. When the effects of DC current on steady-state voltage are equal for both types of neurons, the network remains in a state of synchrony with a pronounced peak at ripple frequency, leading to a high ripple ratio similar to the baseline network conditions (Fig. 3.2A and 3.2B1,B4,B5; mean ripple ratio along the diagonal = 1.20 ± 0.03; n = 11 simulations). Disrupting this balance by preferentially driving either pyramidal neurons or interneurons leads to a decrease in the ripple ratio. When the drive to pyramidal neurons is greater, total power is increased and peak frequency is decreased (Fig. 3.2B2-3; ripple ratios: Fig. 3.2B2 = 0.3684, Fig. 3.2B3 = 0.6952). On the other hand, when the drive to interneurons is greater, the ripple frequency remains relatively unchanged, and the synchrony and total ripple power is reduced, an effect that becomes more pronounced as the current increases (Fig. 3.2B6-7; ripple ratios: Fig. 3.2B6 = 0.9670, Fig. 3.2B7 = 0.6399).

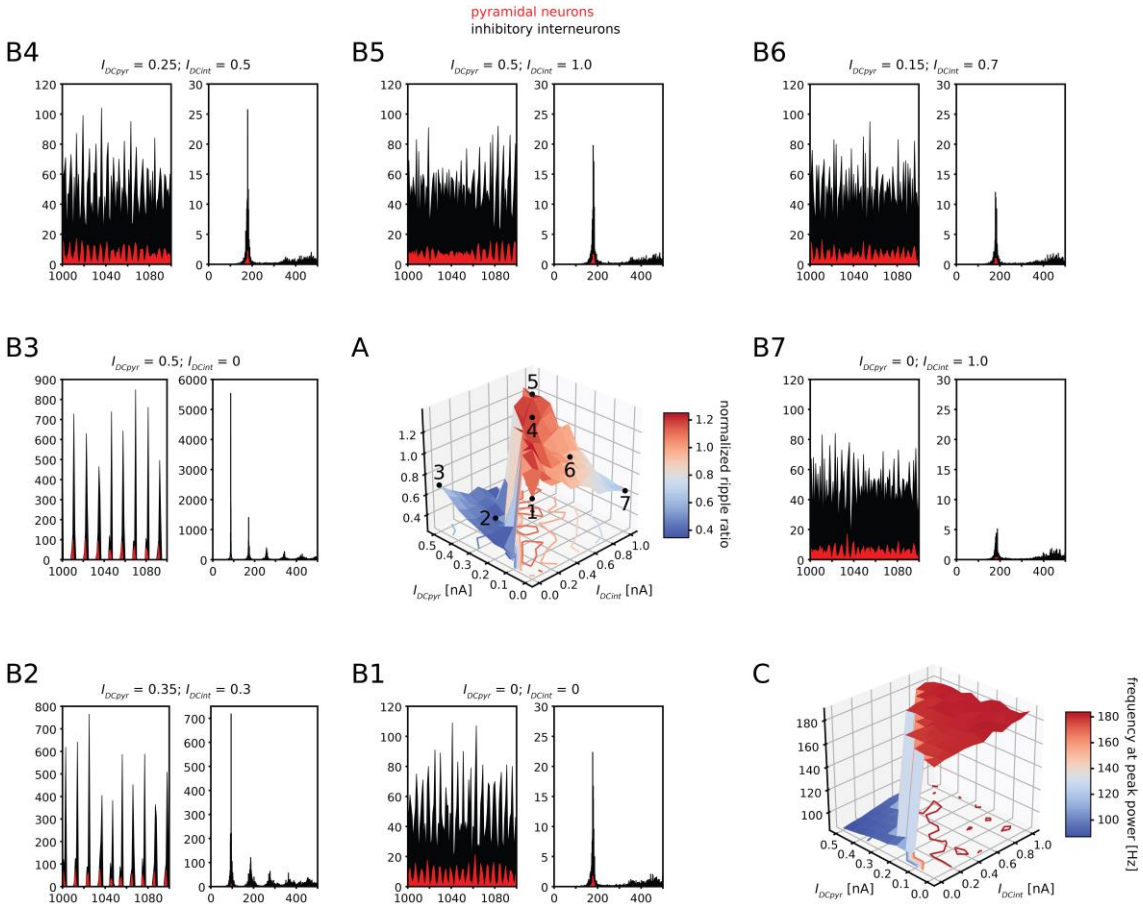

Fig. 3.2. The balance of I_{DC}, a surrogate for cholinergic input from the MS-DB, in both types of neurons determines the resulting effects on ripple ratio and frequency. ***A***: Surface plot showing the ratio of ripple power to low frequency power, normalized to the ratio in the baseline model (see Methods). ***B***: Plots depicting the network rate and power spectra similar to those in Fig. 3.1C. Note that for simulations along the diagonal ridge in ***A***, ripples are preserved (***1***, ***4***, and ***5***), and that points on either side of the ridge are qualitatively similar to other points on their same side (i.e., ***2*** vs. ***3*** and ***6*** vs. ***7***). ***C***: Peak frequencies of the simulations in ***A***. I_{DC} conditions with a larger effect on steady-state voltage in pyramidal neurons cause a drop in peak frequency as compared to those with a larger or equal effect on interneuron steady-state voltage.

Peak frequency also undergoes a change depending on the relative drive to each neuron type. When the DC current to each neuron type lies to the left of the diagonal of the surface plot shown in Fig. 3.2C, meaning there is larger drive to pyramidal neurons than interneurons, an abrupt drop occurs in peak frequency as compared to those simulations on the right of the diagonal (mean peak frequency to the left of the diagonal = 124.17 ± 5.67; n = 55 simulations; mean peak frequency on or to the right of the diagonal = 181.44 ± 0.26; n = 66 simulations). Only when I_{DC} is tuned such that there are equal steady-state voltage changes in both types of neurons does the network obtain both a fast (~180 Hz) ripple frequency and a prominent ripple peak. Thus, responses of the model LFP power with cholinergic-like modulation (through I_{DC}) vary depending on the neuron type being driven. These results, combined with the ripple ratio results above, show that increasing I_{DC} causes three qualitatively different states: (1) increasing primarily I_{DCpyr} results in a lowering of peak frequency and increase in power, (2) increasing primarily I_{DCint} results in a decrease in power and slight increase in peak frequency, and (3) increasing I_{DC} in a balanced manner to both neuron types leads to a preservation of ripples.

3.4.2 I_{DC} drives the network towards one of two types of subnetworks

A two-population network such as the one used here is comprised of two subnetworks: the pyramidal-interneuron-pyramidal (E-I-E) subnetwork, and the interneuron-interneuron (I-I) subnetwork. As these subnetworks are combined, the overall network frequency becomes a compromise between the frequencies of the

constituent E-I-E and I-I loops (Brunel and Wang, 2003). Because of the qualitatively different effects on network oscillations as the neurons are driven to either side of the ridge in Fig. 3.2A, we hypothesized that the imbalance of I_{DC} modulation to one or the other neuron type shifts the overall network towards one of the two subnetworks. Under this hypothesis, increasing drive to pyramidal neurons pushes the network towards the E-I-E loop, while driving interneurons pushes the network towards the I-I loop. In contrast, when drive is balanced, ripples emerge.

To test whether depolarizing inputs push the overall network towards one of the two subnetwork loops, we used two model networks: one consisting solely of E-I and I-E connections (the E-I-E subnetwork, or "no I-I connections") and another consisting solely of interneurons with I-I connections (the I-I subnetwork, or "only I-I connections"). We found that, similar to the results in Brunel and Wang (2003), the E-I-E subnetwork has a peak frequency of 73.26 Hz (Fig. 3.3A; interneuron total ripple power = 39.47 (spikes/neuron)^2), a decrease relative to the original model in Fig. 3.1C. When compared to the effects of increasing I_{DC} only to pyramidal neurons (I_{DCpyr} = 0.5 nA) in the two-population network, the results are similar, with high power and a low peak frequency of 85.68 Hz (Fig. 3.3B; interneuron total ripple power = 23.97 (spikes/neuron)^2). Thus, drive to pyramidal neurons in the original network (with I-I connections intact) works to emphasize the contribution of the E-I-E loop, causing the overall network power spectra to resemble the power spectra of the E-I-E loop in isolation.

We next sought to see if the I-I loop influence could be accentuated with increased drive to interneurons in the original network (with E-I and I-E connections

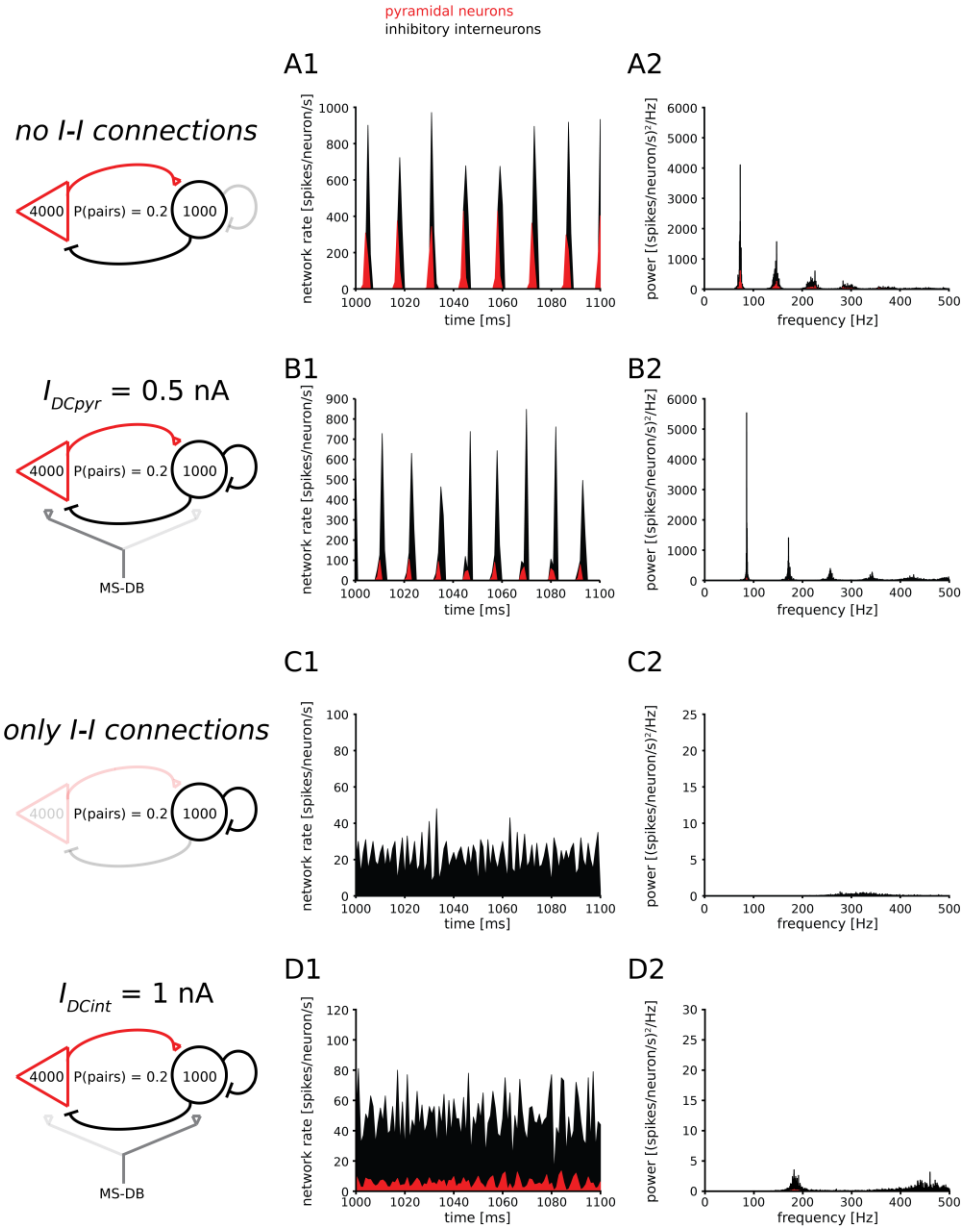

Fig. 3.3. Increases in I_{DCpyr} emphasize the E-I-E network, while increases in I_{DCint} emphasize the I-I network.
Subpanels in ***A***-***D*** show the same analyses as corresponding subpanels in Fig. **3.1*C1*-*C2*** for different network configurations and input current conditions. ***A***: Taken in isolation, the E-I-E network shows high power and a low peak frequency of 73.26 Hz (***2***). ***B:*** The original two-population network with I_{DCpyr} = 0.5 nA also has high power at a low frequency of 85.68 Hz, which is qualitatively similar to the E-I-E network, as shown in ***A***. ***C***: The I-I network (interneuron-only) in isolation shows low power (due to asynchrony) and a broad peak at 276.84 Hz. ***D***: The original two-population network with I_{DCint} = 1 nA also has low power at a slightly higher frequency (relative to baseline) of 182.11 Hz, which is qualitatively similar to the I-I network, as shown in ***C***.

intact). To determine if this is the case, we first observed the ripple power and peak frequency in an interneuron-only network. In keeping with the original two-population network (and deviating from the default parameters for interneuron-only networks in the Methods), we kept the GABAergic synaptic latency (τ_I for GABA or $latency_{GABA}$) of 0.5 ms. This I-I network has a peak frequency of 276.84 Hz (Fig. 3.3C; total ripple power = 0.0508 (spikes/neuron)^2). Similar to the case when pyramidal neurons are driven, driving only interneurons (I_{DCint} = 1 nA) in the original two-population network causes a decrease in power and a slight increase in peak ripple frequency at 182.11 Hz (Fig. 3.3D; interneuron total ripple power = 0.1657 (spikes/neuron)^2). This change is qualitatively similar to the reduction in power and increase in peak frequency (relative to the original two-population network with no I_{DC}) present in the isolated I-I network (Fig. 3.3C).

These results indicate that unbalanced I_{DC} acts to draw out one of two competing subnetworks within the larger network. As drive to one type of neuron increases (resulting from I_{DC}), either the E-I-E subnetwork (in the case of greater I_{DCpyr} increases) or the I-I subnetwork (in the case of greater I_{DCint} increases) dominates, and the resulting power spectrum becomes qualitatively similar to that subnetwork.

3.4.3 Shifts in network frequency can be reversed through preferential input to each neuron type

Our conclusion that I_{DC} alters overall network dynamics by changing the relative contribution of the two subnetworks led us to ask if it is possible to shift the overall network frequency by adjusting the drive to pyramidal neurons and interneurons

following a change in the synaptic parameters of the network. Synaptic parameters, including the latency, rise time, and decay time, determine the peak frequency of the network power spectrum (Brunel and Wang, 2003). Successful shifting of the network frequency following changes to the synaptic parameters would indicate that preferential drive to pyramidal neurons or interneurons can bias network frequency across a range of synaptic parameters and is a robust phenomenon.

In order to test this hypothesis, we shifted the peak frequency of the two-population network, and then sought to correct the shift by driving one of the subnetworks. Peak frequency was first either raised or lowered by changing the synaptic latency time constants of the network. By increasing the synaptic latency, we could achieve lower network frequencies, and by decreasing the synaptic latency, we could achieve higher network frequencies. Then, we opposed the shift in network frequency by driving either the E-I-E subnetwork (the slower loop) or the I-I subnetwork (the faster loop) through depolarization of pyramidal neurons or interneurons, respectively.

We first ran an interneuron-only model of ripples with $latency_{GABA}$ = 1 ms (Fig. 3.4A; default parameters, see Methods). This model has a ripple frequency of 173.89 Hz (interneuron total ripple power = 1.1186 (spikes/neuron)^2). Then, using the two-population original model with no I_{DC} input, we raised $latency_{GABA}$ from 0.5 to 1 ms, such that the ripple peak frequency is reduced, with a ripple frequency of 140.74 Hz (Fig. 3.4B; interneuron total ripple power = 4.4745 (spikes/neuron)^2). Because the I-I network has a higher peak frequency, and I_{DCint} causes the network to behave closer to the I-I loop, we expected I_{DCint} to have a restorative effect, raising ripple frequency from 140.74 Hz to be more similar to the interneuron-only network in Fig. 3.4A. Indeed,

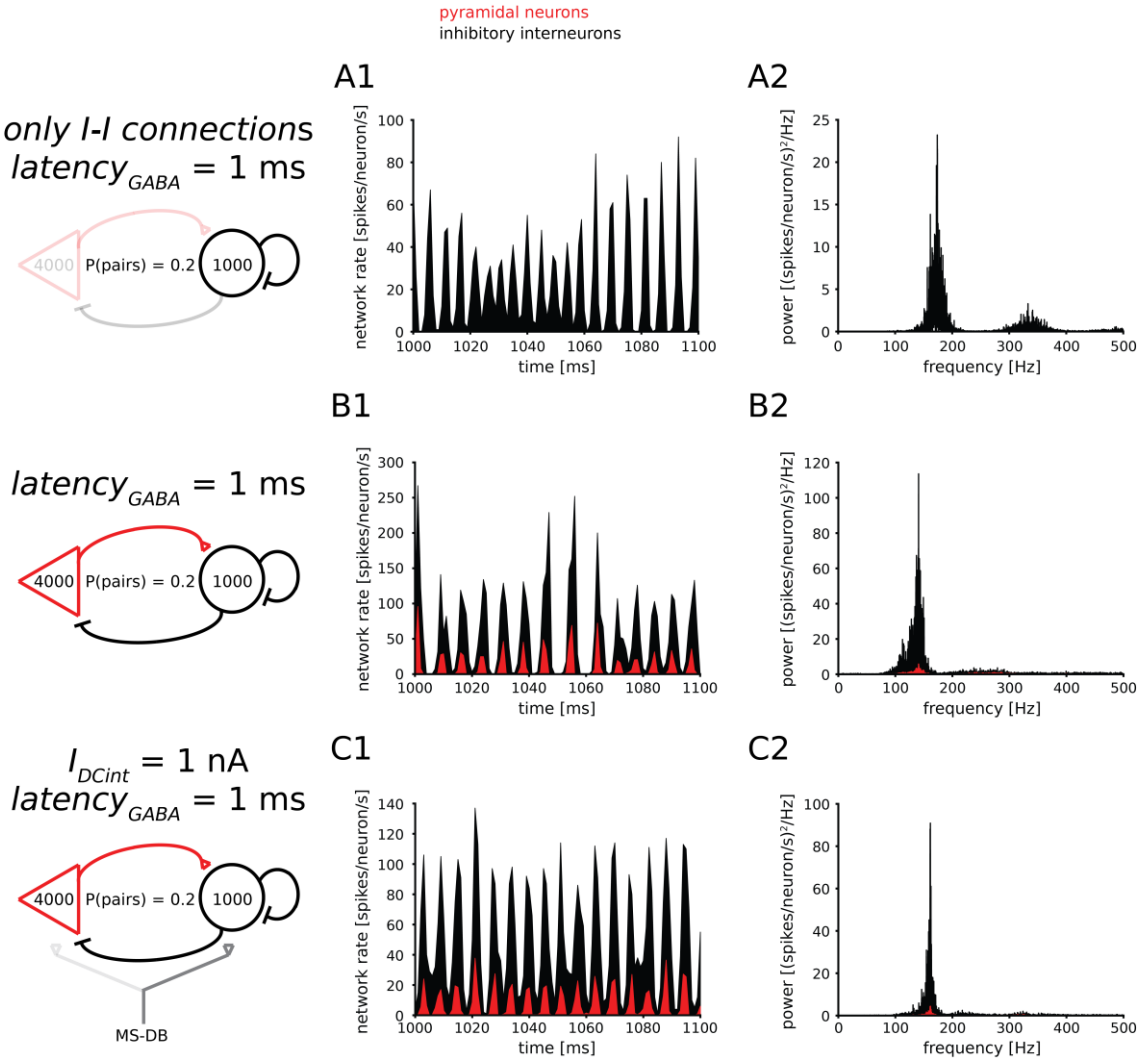

Fig. 3.4. The frequency of a network with a slower GABAergic time constant can be raised with increased drive to the I-I subnetwork.
A: The interneuron-only network with *latency*$_{GABA}$ = 1 ms shows total ripple power and frequency similar to the original network with both neuron types. ***B***: Changing the *latency*$_{GABA}$ of the original network from 0.5 to 1 ms to match the interneuron-only network decreases peak ripple frequency. ***C***: Increasing I_{DCint} to 1 nA draws out the faster I-I loop, raising peak ripple frequency and countering the effect of increasing *latency*$_{GABA}$.

using I_{DCint} = 1 nA leads to an increase in the ripple frequency of the two-population network, with a new overall ripple frequency of 161.37 Hz (Fig. 3.4C; interneuron total ripple power = 2.5587 (spikes/neuron)^2).

In the original two-population network, high ripple ratios and ripple peak frequencies (~180 Hz) are maintained by driving pyramidal cells and interneurons in balance (hence the ridge along the middle of the surface plot in Fig. 3.2A). Changes to the synaptic time constants shift the overall network ripple ratio and frequency by altering the constituent subnetwork dynamics. Therefore, we hypothesized that the overall network could be restored to a high ripple ratio and ripple peak frequency using new values of I_{DC} that are not necessarily balanced.

To probe whether I_{DC} can be used to reestablish a network under different synaptic conditions that generates ripples, we used the same analyses as in Fig. 3.2 and looked at the ripple ratio and frequency across a range of I_{DC} to both pyramidal neurons and interneurons. As shown in Fig. 3.4B, when $latency_{GABA}$ is increased to 1 ms, the network frequency is slowed to 140.74 Hz. Under these conditions, we found that driving the network towards the slower E-I-E loop (by driving pyramidal neurons) tends to decrease the ripple ratio and peak frequency (Figs. 3.5A1 and A2, respectively; I_{DCpyr} = 0.5 nA, I_{DCint} = 0 nA: ripple ratio = 0.2819, ripple frequency = 88.21 Hz; baseline ripple frequency = 141.47 Hz). On the other hand, as also shown in Fig. 3.5A, driving the network towards the I-I loop (by driving interneurons) tends to increase the ripple ratio and frequency (I_{DCpyr} = 0 nA, I_{DCint} = 1 nA: ripple ratio = 2.4182, ripple frequency = 161.37 Hz). These results show that raising the synaptic time constant removes the ridge of high ripple ratios found in the original network (Fig. 3.2A) and instead moves

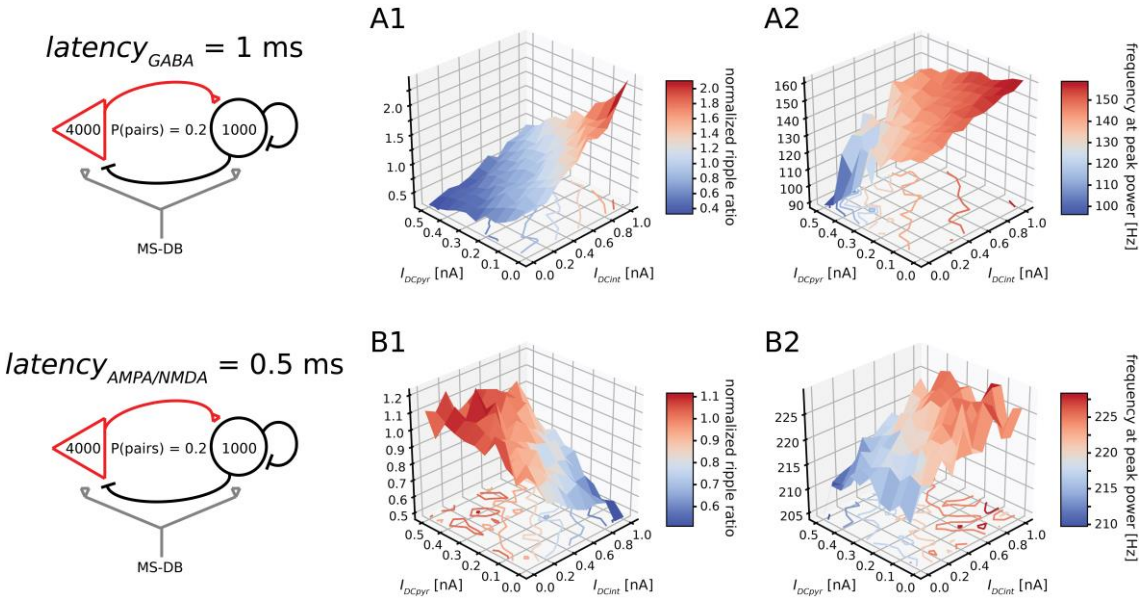

Fig. 3.5. In networks with varied intrinsic frequencies, preferential input to each neuron type can adjust overall network frequency.
A: When ripple frequency is decreased by raising *latency*$_{GABA}$ from 0.5 to 1 ms, increasing I_{DCint} increases ripple ratio (***1***) and frequency (***2***), whereas increasing I_{DCpyr} has the opposite effect. ***B***: When ripple frequency is increased by lowering *latency*$_{AMPA/NMDA}$ from 1 to 0.5 ms, increasing I_{DCpyr} increases ripple ratio (***1***) and slows down the peak oscillation frequency (***2***). Increasing I_{DCint} has the opposite effect.

the location of drive that generates ripples towards interneurons and the I-I loop.

Since changing the synaptic time constants to slow the network can be counteracted by increasing DC drive to interneurons, we next investigated whether the opposite was also true; driving pyramidal neurons can slow an overall network frequency that has been increased by changes to the synaptic time constants. In order to test this hypothesis, we sped up the two-population network by decreasing $latency_{AMPA/NMDA}$ from 1 ms to 0.5 ms (while $latency_{GABA}$ = 0.5 ms). Without any I_{DC} input, this network oscillates with an elevated peak ripple frequency of 218.84 Hz (interneuron total ripple power = 0.7302 (spikes/neuron)^2). We then measured the effects of I_{DCpyr} and I_{DCint} on the ripple ratio and frequency. As expected, the ripple ratio is increased, and the ripple frequency is lowered through driving the slower E-I-E subnetwork by increasing I_{DCpyr} (Fig. 3.5B1 and B2; I_{DCpyr} = 0.5 nA, I_{DCint} = 0 nA: ripple ratio = 1.1116, ripple frequency = 204.11 Hz). Conversely, driving the faster I-I subnetwork by increasing I_{DCint} exacerbates the increase in peak frequency (I_{DCpyr} = 0 nA, I_{DCint} = 1 nA: ripple ratio = 0.4743, ripple frequency = 226.21 Hz). Thus, lowering the synaptic time constant also moves the location of drive that generates ripples, this time towards pyramidal neurons and the E-I-E loop.

In both cases, the shift in peak frequency caused by changes in synaptic parameters is canceled by I_{DC} that drives the subnetwork with an opposing peak frequency bias. On the other hand, the peak frequency shift is intensified by I_{DC} driving the subnetwork with a similar peak frequency bias. These results show that, across a range of synaptic parameters, preferential drive to pyramidal neurons or interneurons can shift network frequency.

3.5 Discussion

We present evidence that changes in the balance of DC current driving hippocampal pyramidal neurons and interneurons can shift the peak frequency and power of ripple oscillations, favoring either the E-I-E loop or the I-I loop. This holds true for a variety of synaptic time constants, and may represent a means whereby hippocampal rhythms are modulated.

3.5.1 Implications for hippocampal ripple modulation by ACh

Our results suggest that a possible mechanism for the disruption of ripples may be the promotion of an asynchronous subnetwork by cholinergic input. As an illustration of this possibility, consider the case of the interneuron-only network proposed by Brunel and Wang (2003): this network displayed a synchronous ~174 Hz oscillation (Fig. 3.4A), likely due to the long synaptic latency of $latency_{GABA}$ = 1 ms (Brunel et al., 2001). In the case of the original two-population network shown in Fig. 3.1C, however, they used a shorter synaptic latency of $latency_{GABA}$ = 0.5 ms in order to increase the frequency of the I-I loop and pull the network away from the slower E-I-E loop. The result is a synchronous ripple oscillation that is present when drive to both neuron types is balanced, but absent when the drive promotes the I-I subnetwork or when pyramidal neurons are eliminated altogether (Figs. 3.3D and C, respectively). This occurs because the shorter $latency_{GABA}$ increases the peak frequency, but decreases ability to follow oscillating input, leading to asynchrony (Brunel et al., 2001). Similarly, ACh stimulation may suppress synchronous ripple oscillations through an input imbalance that draws out a subnetwork which, on its own, is asynchronous. The issue of

balanced excitation and inhibition during ripples has also been shown *in vivo* (English et al., 2014), and the converse may also be true: imbalance between excitation and inhibition may disrupt ripples. This hypothesis could be tested by observing the effect of increasing the relative contribution of the I-I subnetwork on ripple incidence. One possible way to accomplish this would be through optogenetic inhibition of pyramidal neurons, or excitation of interneurons.

In the specific example we just explored, the difference in synaptic latency caused a network to switch from a synchronous to asynchronous oscillation. It is also possible that cholinergic input affects synaptic latency times directly (i.e., the time between a presynaptic spike and a postsynaptic event). Presynaptic nicotinic ACh receptors enhance synaptic transmission in the brain (McGehee et al., 1995), including in hippocampal neurons (Gray et al., 1996; Boudkkazi et al., 2007; Zhong et al., 2013). An increase in the probability of vesicle release also decreases the average release latency time (Boudkkazi et al., 2007). Supporting this possibility is a range of GABAergic synaptic latencies in CA1 (0.68 ± 0.03 ms between basket cells, and 0.9 ± 0.1 ms between basket cells and pyramidal neurons; Bartos et al., 2002). Differences in synaptic latencies between neuron types involved in different hippocampal subnetworks also opens the door to cholinergic suppression of ripples through subnetwork activation.

3.5.2 Accuracy of the simplified model of cholinergic suppression of ripples

The network used here was chosen because of its popularity in the field (Buzsáki et al., 2004; Buzsáki, 2006; Bartos et al., 2007; Ray and Maunsell, 2011) and

because it replicates the biological phenomena we were studying: the model reproduces ripple activity in a network with realistic connectivity and synaptic parameters. In this network, interneurons lag behind pyramidal neurons (Maier et al., 2011; Hulse et al., 2016), and similar to biological neurons *in vivo* (English et al., 2014; Hulse et al., 2016), model neurons showed an average voltage oscillation at ripple frequencies that went away as ripple power decreased (data not shown).

Alternative models to the one by Brunel and Wang (2003) have also been used to study hippocampal ripples (Traub et al., 1999; Traub and Bibbig, 2000; Malerba et al., 2016). Using the ripple model proposed by Malerba et al., however, we used struggled to reproduce the suppression of ripples following increases in input current to pyramidal neurons and interneurons (data not shown; Malerba et al., 2016). Another popular model suggests that hippocampal ripples can be generated in pyramidal neurons with axo-axonal gap junctions (Traub et al., 1999; Traub and Bibbig, 2000). This model features ectopic spikes that propagate antidromically. In contrast, recent studies have shown that, during ripples, spikes in hippocampal neurons propagate orthodromically (English et al., 2014; Hulse et al., 2016). In order to avoid these complications, we chose to use a model that both shows a decrease in ripple power with cholinergic-like depolarization (I_{DC}) and uses chemical synapses to generate ripples. Although a more detailed model of cholinergic input would be preferable to I_{DC}, we were unable to find sufficient quantitative details about the kinetics of the cholinergic response in the literature. Nevertheless, the model we used makes predictions that are experimentally verifiable using recently developed techniques, such as the ability to selectively drive different neuron types during ripple oscillations.

Our decision to focus on membrane depolarization excluded the other effects of cholinergic input to hippocampal neurons. As mentioned previously, the effects of ACh on membrane resistance and AHP vary widely, especially among different interneuron cell types. Furthermore, adaptation was not included because typical adaptation timescales are >100 ms (Fleidervish et al., 1996; Fernandez and White, 2009, 2010), whereas typical ripple events have a duration of about 50 ms (Malerba et al., 2016). Therefore, although we cannot rule out these effects as being necessary for the cholinergic suppression of ripples, we did not include them in our study.

One particularly important feature of the model we used was the individual interneuron mean firing rate of ~50 Hz. Our previous work has shown that gain modulation in cholinergic MS-DB neurons is possible with hyperpolarization (Melonakos et al., 2016), and hippocamposeptal (somatostatin$^+$ GABAergic) neurons most effectively evoke hyperpolarization in cholinergic MS-DB neurons when driven at 50 Hz (Mattis et al., 2014). Since optogenetic activation of cholinergic MS-DB neurons blocks ripples in the hippocampus, while increasing theta power and coherence (Vandecasteele et al., 2014), it would be interesting to see if 50 Hz somatostatin$^+$ GABAergic neuron firing could reduce gain in cholinergic neurons, reducing their output and increasing the incidence of ripples. This could be studied in a model of the complete septohippocampal loop. Currently, the relationship between cholinergic MS-DB neuron firing rates and the postsynaptic effects of ACh is not known. Future studies that address this gap would make it possible to recreate a more complete model of the septohippocampal control loop.

CHAPTER 4

DISCUSSION

4.1 Summary of results

The role of MS-DB neurons in hippocampal rhythms continues to be a matter of widespread interest. Among the most influential neuron types in these rhythms are cholinergic neurons. In this dissertation, we have explored the intrinsic membrane properties of these neurons and sought to explain how these properties might affect their role in both hippocampal theta and sharp wave-ripples.

4.1.1 Cholinergic neuron response to hyperpolarizing inputs

Cholinergic neurons in the MS-DB receive hyperpolarizing inputs from hippocamposeptal inhibitory neurons (Alonso and Köhler, 1982; Tóth et al., 1993; Dragoi et al., 1999; Gulyás et al., 2003; Jinno et al., 2007; Takács et al., 2008; Mattis et al., 2014). The response of cholinergic MS-DB neurons to such inputs depends upon their intrinsic membrane properties. In Chapter 2, we compared these properties in both cholinergic neurons and noncholinergic neurons, starting with the membrane resistance, capacitance, and time constant at subthreshold voltages. We found no significant differences in the subthreshold membrane properties between different neuron types in the MS-DB. This result suggests that differences in the spike outputs of these neurons are

not determined by differences in their subthreshold membrane properties. We also measured the responses of the neurons following hyperpolarizing inputs, finding a marked reduction in the firing rate and gain of cholinergic neurons. These results were specific to cholinergic neurons, and there was no effect of hyperpolarization on noncholinergic neurons (presumably GABAergic). Furthermore, we used voltage-clamp to measure and characterize a slowly activating and inactivating K^+ current in cholinergic neurons. Consistent with the similarities between cholinergic and noncholinergic subthreshold membrane properties, this current activates only at suprathreshold voltages. In combination with an experimentally verified shallow *f-V* curve, depolarization following hyperpolarization leads to activation of the K^+ current, which increases its activation with increasing firing rate and depolarization. Together, these factors account for the reduction in gain following hyperpolarization.

The results from Chapter 2 expand upon previous results describing cholinergic MS-DB neurons as slow-spiking (Griffith and Matthews, 1986; Markram and Segal, 1990; Simon et al., 2006); we show that the slow firing rate and responsiveness of these cells is critically dependent on the state of membrane voltage preceding their activation. Although others have shown data consistent with the presence of a slowly inactivating K^+ current in MS-DB neurons (Garrido-Sanabria et al., 2011), our work confirms and describes the magnitude and kinetics of this current in detail, as well as its effect on input-output curves. Also, our results showing that gain reductions through the slowly inactivating K^+ current depend on a shallow *f-V* curve are consistent with recent results in Patel and Burdakov (2015). Overall, our work in Chapter 2 answers key questions about the response of cholinergic MS-DB neurons to inhibitory input and provides a proof-of-

concept concerning the interactions of voltage-dependent conductances and neuronal *f-V* curves.

4.1.2 Mechanism of cholinergic suppression of hippocampal ripples

Hippocampal ripples occur during slow-wave sleep and immobility (O'Keefe, 1976; Buzsáki et al., 1983, 1992), and are important for the encoding of future experience (Dragoi and Tonegawa, 2012) and the consolidation of past experiences (Wilson and McNaughton, 1994; Davidson et al., 2009; Girardeau et al., 2009). Ripples are silenced by input from cholinergic MS-DB neurons (Vandecasteele et al., 2014), and they coincide with a decrease in MS-DB neuron firing (Dragoi et al., 1999). In Chapter 3, we explored the effects of cholinergic-like modulation of hippocampal neurons in a ripple-generating model network. We presented evidence that ripple power and frequency can be shifted through changes in the balance of drive to different hippocampal neuron types. The relative drive balance between the different neuron types either promotes the slower pyramidal-interneuron-pyramidal subnetwork or the faster interneuron-interneuron subnetwork. Our results suggest the possible modulation of hippocampal rhythms through this mechanism. Specifically, cholinergic drive may disrupt ripples by promoting asynchronous subnetworks.

The work presented in Chapter 3 fills a gap in the scientific literature by linking the cellular effects of cholinergic modulation of hippocampal neurons with the effects of cholinergic modulation of network rhythms. Although numerous studies have observed and measured the effects of cholinergic modulation on hippocampal pyramidal neurons

(Dodd et al., 1981; Benardo and Prince, 1982; Cole and Nicoll, 1984; Madison and Nicoll, 1984) and interneurons (Chapman and Lacaille, 1999; McQuiston and Madison, 1999a; b; c), none of these studies provide a mechanistic explanation for the cholinergic suppression of ripples. Our results support previous findings showing balanced excitation and inhibition in hippocampal neurons during ripple oscillations (English et al., 2014) and present imbalanced cholinergic drive as a possible mechanism for ripple suppression.

Together, Chapters 2 and 3 focus on the role of cholinergic neurons in the septohippocampal circuit. They lay groundwork for future experimental and modeling studies that explore (1) the effect of gain changes in cholinergic MS-DB neurons, and (2) the influence of cholinergic modulation on balanced excitation and inhibition in hippocampal neurons during hippocampal rhythms.

4.2 Effects of gain changes in cholinergic MS-DB neurons on neural rhythms

As mentioned in Chapter 1, hippocampal theta rhythms and sharp wave-ripples share a dichotomous relationship regarding the behaviors during which they occur (Buzsáki, 2015). These two rhythms also exhibit opposite responses to cholinergic input (Vandecasteele et al., 2014). Due to the differing responses of hippocampal theta and ripples to cholinergic input, changes in the sensitivity of cholinergic neurons to inputs may affect the downstream hippocampal oscillations.

As shown in Chapter 2, hyperpolarization of cholinergic MS-DB neurons causes a long-lasting reduction in firing rate and gain. Input to cholinergic MS-DB neurons comes from multiple sources: local GABAergic and glutamatergic neurons provide inhibitory

and excitatory inputs, respectively (Colom et al., 2005; Leão et al., 2015); hypothalamic inputs provide excitatory drive (Gerashchenko et al., 2001); hippocamposeptal neurons provide inhibitory feedback (Alonso and Köhler, 1982; Tóth et al., 1993; Dragoi et al., 1999; Gulyás et al., 2003; Jinno et al., 2007; Takács et al., 2008; Mattis et al., 2014). The relay of inputs from cholinergic MS-DB neurons to hippocampal pyramidal and basket neurons may influence hippocampal theta. For this reason, modulation of cholinergic MS-DB neuron gain may change the hippocampal oscillatory state.

Under this hypothesis, high cholinergic MS-DB neuron gain increases the amount of cholinergic drive to hippocampal neurons. Conversely, low cholinergic MS-DB neuron gain decreases the amount of cholinergic drive hippocampal neurons, thus decreasing theta amplitude and increasing the likelihood of ripples. The influence of cholinergic MS-DB neuronal gain changes may also extend to local connections with other MS-DB neurons, indirectly influencing hippocampal rhythms.

Hippocampal oscillations may exert some control over hyperpolarization, and thus gain reduction, in cholinergic MS-DB neurons. Long-lasting hyperpolarization of cholinergic MS-DB neurons is most pronounced following ripple frequency stimulation of hippocamposeptal neurons (50 Hz, or the spike frequency of some interneurons during ripples) (Mattis et al., 2014). Less effective hyperpolarization is evoked following stimulation of hippocamposeptal neurons at theta frequency (8 Hz). Inversely, stimulation of cholinergic MS-DB neurons at theta-like frequencies (1-12 Hz) results in dramatic suppression of hippocampal ripples (Vandecasteele et al., 2014). Taken together with our results, these findings indicate that hippocampal ripples prevent their own suppression by silencing cholinergic MS-DB neurons.

We also propose that the gain of these neurons can be changed as a result of the hyperpolarization that comes with high frequency hippocampal activity. Indeed, during ripples, firing in the majority of medial septal neurons is suppressed (Dragoi et al., 1999). Thus, hippocamposeptal neurons could *dis*inhibit ripples by suppressing cholinergic MS-DB neuronal activity. This would provide a mechanism whereby the hippocampus could provide feedback to the MS-DB, forcing the excitability of cholinergic neurons to alternate with hippocampal ripples.

Future models of the entire septohippocampal loop would provide a means to explore the role of cholinergic neurons in the loop. A model that includes both MS-DB neurons reciprocally connected to the hippocampus and hippocampal rhythms would allow exploration of the effects of gain modulation on downstream network oscillations. Ideally, a model such as this would contain detailed cholinergic MS-DB neurons, including the ability for hyperpolarization-induced gain reductions.

One possible model for this type of loop is the Brunel and Wang (2003) model we used in Chapter 3. In addition to this model, a variety of others have been proposed in the literature, including axo-axonic gap junction models (Traub et al., 1999; Traub and Bibbig, 2000) and other chemical synapse-based models (Taxidis et al., 2012). Each of these model types focuses on a different aspect of ripples, and each could thus help answer different questions about the septohippocampal loop.

Models of the septohippocampal loop should also include cholinergic MS-DB neurons similar to the eLIF model we described in Chapter 2 of this work. Because of the results presented in that chapter, these model neurons use experimentally measured membrane parameters and currents, including the slowly inactivating K^+ current.

Furthermore, muscarinic and nicotinic input to hippocampal pyramidal and GABAergic neurons could be modeled using the distributions found in Teles-Grilo Ruivo and Mellor (2013) and the experimental results from Cole and Nicoll (1984) and others described in Chapter 3. Unlike the DC current modulation we used in Chapter 3, a mathematical description of the kinetics and magnitude of cholinergic input would increase the accuracy of these models. Therefore, studies revealing the quantitative details of cholinergic postsynaptic events could advance our ability to model the septohippocampal circuit. In addition, the functional relationship between cholinergic MS-DB neuron spike output and cholinergic input to hippocampal neurons is necessary. Future studies that address these knowledge gaps would allow for the recreation of the septohippocampal control loop *in silico*.

One way to validate potential model networks would be to replicate the result from Vandecasteele et al. (2014) by observing whether ripples are disrupted following 1-12 Hz cholinergic input onto model hippocampal neurons. If successful, our hypothesis that hyperpolarization-induced gain changes are critical for ripple disruption could then be tested by comparing simulations with and without the slowly inactivating K^+ current. Furthermore, the degree to which gain impacts ripple disinhibition could be determined by shifting the activation curve of the K^+ conductance to vary its overlap with the suprathreshold voltage range (Patel and Burdakov, 2015). Through this method, the degree to which the slowly inactivating K^+ current impacts gain could be systematically altered and the resulting effect on ripple disinhibition could be measured.

Future *in vivo* experiments that test these hypotheses will also be needed to confirm the expected results of these proposed models. If the models are correct, and if

hyperpolarization-induced gain reductions in cholinergic MS-DB neurons are required for proper ripple function, then selective block of the slowly inactivating K^+ current may lead to learning deficits due to impaired ripples and memory consolidation. In addition, the ability to target genetically diverse populations of neurons *in vivo* makes it possible to observe the effects of hyperpolarization on input-output properties of neurons through selective stimulation. This could be done through optogenetic stimulation of inhibitory hippocamposeptal neurons, followed by measurements of cholinergic neuron gain and ripple incidence.

4.3 The role of balanced excitation and inhibition in hippocampal rhythms

During hippocampal ripples, large depolarizations in pyramidal neurons are matched by inhibition, which results in a balancing of excitation and inhibition (English et al., 2014). The balance between excitatory and inhibitory synaptic currents is key in determining the network frequency in populations of pyramidal neurons and interneurons (Brunel and Wang, 2003). As such, our results in Chapter 3 present a possible mechanism for alternating between different hippocampal rhythms, including ripples and theta; cholinergic input may promote subnetworks that reduce ripples and promote theta by causing an imbalance between the previously balanced excitation and inhibition. To test this hypothesis, future studies could measure the effect of selectively driving pyramidal neurons or various interneuron subtypes during ripple oscillations, thus increasing the relative activation level of the E-I-E loop or the I-I loop, respectively. Studies such as McQuiston and Madison (1999a; c), which describe the various effects of cholinergic

input to different types of interneurons, are invaluable in informing experiments such as the one just proposed.

In support of the theory that cholinergic modulation disrupts the balance between excitation and inhibition, one study showed that optogenetically activating hippocampal parvalbumin-positive interneurons causes theta-frequency spiking in pyramidal neurons (Stark et al., 2013). Thus, shifting the balance of drive to interneurons may allow the frequency of the network to shift to the theta range. Our modeling results in Chapter 3 also generated a decrease in ripple power when interneurons are driven, highlighting the opposing responses of hippocampal theta and ripples to cholinergic modulation. Therefore, the results in Stark et al. (2013) combined with our results suggest that it may be possible for cholinergic input to hippocampal neurons to simultaneously promote theta and suppress ripples.

In this dissertation, we have presented results describing the integration properties of cholinergic neurons in the MS-DB and a possible mechanism whereby cholinergic drive from these neurons may silence hippocampal ripple oscillations. This research may motivate future experiments and models that advance our understanding of the role of cholinergic modulation in the septohippocampal loop in facilitating learning and memory.

REFERENCES

Aggleton JP, Hunt PR, Rawlins JN. 1986. The effects of hippocampal lesions upon spatial and non-spatial tests of working memory. Behav Brain Res 19:133–46.

Alonso A, Köhler C. 1982. Evidence for separate projections of hippocampal pyramidal and non-pyramidal neurons to different parts of the septum in the rat brain. Neurosci Lett 31:209–14.

Atri A, Sherman S, Norman KA, Kirchhoff BA, Nicolas MM, Greicius MD, Cramer SC, Breiter HC, Hasselmo ME, Stern CE. 2004. Blockade of central cholinergic receptors impairs new learning and increases proactive interference in a word paired-associate memory task. Behav Neurosci 118:223–236.

Bartos M, Vida I, Frotscher M, Meyer A, Monyer H, Geiger JRP, Jonas P. 2002. Fast synaptic inhibition promotes synchronized gamma oscillations in hippocampal interneuron networks. Proc Natl Acad Sci U S A 99:13222–13227.

Bartos M, Vida I, Jonas P. 2007. Synaptic mechanisms of synchronized gamma oscillations in inhibitory interneuron networks. Nat Rev Neurosci 8:45–56.

Benardo LS, Prince DA. 1982. Ionic mechanisms of cholinergic excitation in mammalian hippocampal pyramidal cells. Brain Res 249:333–344.

Berry SD, Thompson RF. 1978. Prediction of learning rate from the hippocampal electroencephalogram. Science 200:1298–300.

Bezaire MJ, Soltesz I. 2013. Quantitative assessment of CA1 local circuits: Knowledge base for interneuron-pyramidal cell connectivity. Hippocampus 23:751–785.

Boudkkazi S, Carlier E, Ankri N, Caillard O, Giraud P, Fronzaroli-Molinieres L, Debanne D. 2007. Release-dependent variations in synaptic latency: A putative code for short- and long-term synaptic dynamics. Neuron 56:1048–1060.

Brunel N, Chance F, Fourcaud-Trocmé N, Abbott L. 2001. Effects of synaptic noise and filtering on the frequency response of spiking neurons. Phys Rev Lett 86:2186–2189.

Brunel N, Wang X-J. 2003. What determines the frequency of fast network oscillations with irregular neural discharges? I. Synaptic dynamics and excitation-inhibition balance. J Neurophysiol 90:415–30.

Bush D, Barry C, Burgess N. 2014. What do grid cells contribute to place cell firing? Trends Neurosci 37:136–145.

Buzsáki G. 2005. Theta rhythm of navigation: Link between path integration and landmark navigation, episodic and semantic memory. Hippocampus 15:827–40.

Buzsáki G. 2006. Rhythms of the Brain. Oxford University Press.

Buzsáki G. 2015. Hippocampal sharp wave-ripple: A cognitive biomarker for episodic memory and planning. Hippocampus 25:1073–1188.

Buzsáki G, Geisler C, Henze DA, Wang XJ. 2004. Interneuron diversity series: Circuit complexity and axon wiring economy of cortical interneurons. Trends Neurosci 27:186–193.

Buzsáki G, Horvath Z, Urioste R, Hetke J, Wise K. 1992. High-frequency network oscillation in the hippocampus. Science 256:1025–1027.

Buzsáki G, Leung LW, Vanderwolf CH. 1983. Cellular bases of hippocampal EEG in the behaving rat. Brain Res 287:139–71.

Chapman CA, Lacaille J-C. 1999. Cholinergic induction of theta-frequency oscillations in hippocampal inhibitory interneurons and pacing of pyramidal cell firing. J Neurosci 19:8637–8645.

Christian EP, Dudek FE. 1988. Electrophysiological evidence from glutamate microapplications for local excitatory circuits in the CA1 area of rat hippocampal slices. J Neurophysiol 59:110 LP-123.

Chrobak JJ, Buzsáki G. 1996. High-frequency oscillations in the output networks of the hippocampal-entorhinal axis of the freely behaving rat. J Neurosci 16:3056–3066.

Cole AE, Nicoll RA. 1983. Acetylcholine mediates a slow synaptic potential in hippocampal pyramidal cells. Science 221:1299–1301.

Cole AE, Nicoll RA. 1984. Characterization of a slow cholinergic post-synaptic potential recorded *in vitro* from rat hippocampal pyramidal cells. J Physiol 352:173–188.

Colom LV., Castaneda MT, Reyna T, Hernandez S, Garrido-Sanabria ER. 2005. Characterization of medial septal glutamatergic neurons and their projection to the hippocampus. Synapse 58:151–164.

Connor JA, Stevens CF. 1971. Prediction of repetitive firing behaviour from voltage clamp data on an isolated neurone soma. J Physiol 213:31–53.

Connor JA, Walter D, McKown R. 1977. Neural repetitive firing: Modifications of the Hodgkin-Huxley axon suggested by experimental results from crustacean axons. Biophys J 18:81–102.

Csicsvari J, Hirase H, Czurkó A, Mamiya A, Buzsáki G. 1999. Oscillatory coupling of hippocampal pyramidal cells and interneurons in the behaving Rat. J Neurosci 19:274–287.

Csicsvari J, Hirase H, Mamiya A, Buzsáki G. 2000. Ensemble patterns of hippocampal CA3-CA1 neurons during sharp wave-associated population events. Neuron 28:585–594.

Davidson TJ, Kloosterman F, Wilson MA. 2009. Hippocampal replay of extended experience. Neuron 63:497–507.

Dodd J, Dingledine R, Kelly JS. 1981. The excitatory action of acetylcholine on hippocampal neurones of the guinea pig and rat maintained *in vitro*. Brain Res 207:109–127.

Dragoi G, Carpi D, Recce M, Csicsvari J, Buzsáki G. 1999. Interactions between hippocampus and medial septum during sharp waves and theta oscillation in the behaving rat. J Neurosci 19:6191–6199.

Dragoi G, Tonegawa S. 2012. Preplay of future place cell sequences by hippocampal cellular assemblies. Nature 469:397–401.

Dragoi G, Tonegawa S. 2013. Distinct preplay of multiple novel spatial experiences in the rat. Proc Natl Acad Sci U S A 110:9100–5.

Dragoi G, Tonegawa S. 2014. Selection of preconfigured cell assemblies for representation of novel spatial experiences. Philos Trans R Soc Lond B Biol Sci 369:20120522.

Easton A, Ridley RM, Baker HF, Gaffan D. 2002. Unilateral lesions of the cholinergic basal forebrain and fornix in one hemisphere and inferior temporal cortex in the opposite hemisphere produce severe learning impairments in rhesus monkeys. Cereb Cortex 12:729–736.

English DF, Peyrache A, Stark E, Roux L, Vallentin D, Long MA, Buzsáki G. 2014. Excitation and inhibition compete to control spiking during hippocampal ripples: Intracellular study in behaving mice. J Neurosci 34:16509–16517.

Fernandez FR, White JA. 2009. Reduction of spike afterdepolarization by increased leak conductance alters interspike interval variability. J Neurosci 29:973–86.

Fernandez FR, White JA. 2010. Gain control in CA1 pyramidal cells using changes in somatic conductance. J Neurosci 30:230–41.

Figenschou A, Hu G-Y, Storm JF. 1996. Cholinergic modulation of the action potential in rat hippocampal neurons. Eur J Neurosci 8:211–219.

Fleidervish IA, Friedman A, Gutnick MJ. 1996. Slow inactivation of Na^+ current and

slow cumulative spike adaptation in mouse and guinea-pig neocortical neurones in slices. J Physiol 493.1:83–97.

Fox SE, Wolfson S, Ranck JB. 1986. Hippocampal theta rhythm and the firing of neurons in walking and urethane anesthetized rats. Exp brain Res 62:495–508.

Frazier CJ, Rollins YD, Breese CR, Leonard S, Freedman R, Dunwiddie TV. 1998. Acetylcholine activates an alpha-bungarotoxin-sensitive nicotinic current in rat hippocampal interneurons, but not pyramidal cells. J Neurosci 18:1187–1195.

Fries P, Reynolds JH, Rorie AE, Desimone R. 2001. Modulation of oscillatory neuronal synchronization by selective visual attention. Science 291:1560–3.

Fuhrmann F, Justus D, Sosulina L, Kaneko H, Beutel T, Friedrichs D, Schoch S, Schwarz MKM, Fuhrmann M, Remy S. 2015. Locomotion, theta oscillations, and the speed-correlated firing of hippocampal neurons are controlled by a medial septal glutamatergic circuit. Neuron 86:1253–1264.

Garrido-Sanabria ER, Perez-Cordova MG, Colom LV. 2011. Differential expression of voltage-gated K^+ currents in medial septum/diagonal band complex neurons exhibiting distinct firing phenotypes. Neurosci Res 70:361–9.

Gerashchenko D, Salin-Pascual R, Shiromani PJ. 2001. Effects of hypocretin-saporin injections into the medial septum on sleep and hippocampal theta. Brain Res 913:106–15.

Girardeau G, Benchenane K, Wiener SI, Buzsáki G, Zugaro MB. 2009. Selective suppression of hippocampal ripples impairs spatial memory. Nat Neurosci 12:1222–1223.

Goutagny R, Krantic S. 2013. Hippocampal oscillatory activity in Alzheimer's disease: toward the identification of early biomarkers? Aging Dis 4:134–40.

Gray R, Rajan AS, Radcliffe KA, Yakehiro M, Dani JA. 1996. Hippocampal synaptic transmission enhanced by low concentrations of nicotine. Nature 383:713–716.

Griffith WH, Matthews RT. 1986. Electrophysiology of AChE-positive neurons in basal forebrain slices. Neurosci Lett 71:169–174.

Griffith WH, Sim JA. 1990. Comparison of 4-aminopyridine and tetrahydroaminoacridine on basal forebrain neurons. J Pharmacol Exp Ther 255:986–993.

Gulyás AI, Hajos N, Katona I, Freund TF. 2003. Interneurons are the local targets of hippocampal inhibitory cells which project to the medial septum. Eur J Neurosci 17:1861–1872.

Hafting T, Fyhn M, Molden S, Moser M, Moser EI. 2005. Microstructure of a spatial

map in the entorhinal cortex. Nature 436:801–806.

Harvey CD, Collman F, Dombeck DA, Tank DW. 2009. Intracellular dynamics of hippocampal place cells during virtual navigation. Nature 461:941–6.

Hasselmo ME. 2005. What is the function of hippocampal theta rhythm?—Linking behavioral data to phasic properties of field potential and unit recording data. Hippocampus 15:936–49.

Heath NC, Rizwan AP, Engbers JDT, Anderson D, Zamponi GW, Turner RW. 2014. The expression pattern of a Cav3-Kv4 complex differentially regulates spike output in cerebellar granule cells. J Neurosci 34:8800–12.

Hirase H, Czurkó A, Csicsvari J, Buzsáki G. 1999. Firing rate and theta-phase coding by hippocampal pyramidal neurons during "space clamping." Eur J Neurosci 11:4373–4380.

Hulse BK, Moreaux LC, Lubenov EV., Siapas AG. 2016. Membrane potential dynamics of CA1 pyramidal neurons during hippocampal ripples in awake mice. Neuron 89:800–813.

Ji D, Wilson MA. 2007. Coordinated memory replay in the visual cortex and hippocampus during sleep. Nat Neurosci 10:100–107.

Jinno S, Klausberger T, Marton LF, Dalezios Y, Roberts JDB, Fuentealba P, Bushong EA, Henze D, Buzsáki G, Somogyi P. 2007. Neuronal diversity in GABAergic long-range projections from the hippocampus. J Neurosci 27:8790–8804.

Justus D, Dalügge D, Bothe S, Fuhrmann F, Hannes C, Kaneko H, Friedrichs D, Sosulina L, Schwarz I, Anthony Elliott D, Schoch S, Bradke F, Karl Schwarz M, Remy S. 2017. Glutamatergic synaptic integration of locomotion speed via septoentorhinal projections. Nat Neurosci 20:16–19.

Kramis R, Vanderwolf CH, Bland BH. 1975. Two types of hippocampal rhythmical slow activity in both the rabbit and the rat: Relations to behavior and effects of atropine, diethyl ether, urethane, and pentobarbital. Exp Neurol 49:58–85.

Lawson VH, Bland BH. 1993. The role of the septohippocampal pathway in the regulation of hippocampal field activity and behavior: Analysis by the intraseptal microinfusion of carbachol, atropine, and procaine. Exp Neurol 120:132–144.

Leão RN, Targino ZH, Colom LV., Fisahn A. 2015. Interconnection and synchronization of neuronal populations in the mouse medial septum/diagonal band of Broca. J Neurophysiol 113:971–980.

Lee MG, Chrobak JJ, Sik A, Wiley RG, Buzsáki G. 1994. Hippocampal theta activity following selective lesion of the septal cholinergic system. Neuroscience 62:1033–1047.

Leutgeb S, Mizumori SJ. 1999. Excitotoxic septal lesions result in spatial memory deficits and altered flexibility of hippocampal single-unit representations. J Neurosci 19:6661–72.

Logothetis NK, Pauls J, Augath M, Trinath T, Oeltermann A. 2001. Neurophysiological investigation of the basis of the fMRI signal. Nature 412:150–157.

Madison DV., Nicoll RA. 1984. Control of the repetitive discharge of rat CA1 pyramidal neurones *in vitro*. J Physiol 354:319–331.

Magariños-Ascone C, Núñez Á, Delgado-García JM. 1999. Different discharge properties of rat facial nucleus motoneurons. Neuroscience 94:879–886.

Maier N, Tejero-Cantero A, Dorrn AL, Winterer J, Beed PS, Morris G, Kempter R, Poulet JF a, Leibold C, Schmitz D. 2011. Coherent phasic excitation during hippocampal ripples. Neuron 72:137–52.

Maingret N, Girardeau G, Todorova R, Goutierre M, Zugaro MB. 2016. Hippocampo-cortical coupling mediates memory consolidation during sleep. Nat Neurosci 19:959–964.

Malerba P, Krishnan GP, Fellous J-M, Bazhenov M. 2016. Hippocampal CA1 ripples as inhibitory transients. PLOS Comput Biol 12:e1004880.

Manseau F, Goutagny R, Danik M, Williams S. 2008. The hippocamposeptal pathway generates rhythmic firing of GABAergic neurons in the medial septum and diagonal bands : An investigation using a complete septohippocampal preparation *in vitro*. J Neurosci 28:4096–4107.

Markram H, Segal M. 1990. Electrophysiological characteristics of cholinergic and non-cholinergic neurons in the rat medial septum-diagonal band complex. Brain Res 513:171–174.

Mattis J, Brill J, Evans S, Lerner TN, Davidson TJ, Hyun M, Ramakrishnan C, Deisseroth K, Huguenard JR. 2014. Frequency-dependent, cell type-divergent signaling in the hippocamposeptal projection. J Neurosci 34:11769–11780.

McGeer PL, McGeer EG, Suzuki J, Dolman CE, Nagai T. 1984. Aging, Alzheimer's disease, and the cholinergic system of the basal forebrain. Neurology 34:741–5.

McGehee DS, Heath MJ, Gelber S, Devay P, Role LW. 1995. Nicotine enhancement of fast excitatory synaptic transmission in CNS by presynaptic receptors. Science 269:1692–6.

McQuiston AR, Madison DV. 1999a. Muscarinic receptor activity has multiple effects on the resting membrane potentials of CA1 hippocampal interneurons. J Neurosci 19:5703–5710.

McQuiston AR, Madison DV. 1999b. Nicotinic receptor activation excites distinct subtypes of interneurons in the rat hippocampus. J Neurosci 19:2887–2896.

McQuiston AR, Madison DV. 1999c. Muscarinic receptor activity induces an afterdepolarization in a subpopulation of hippocampal CA1 interneurons. J Neurosci 19:5703–5710.

Melonakos ED, White JA, Fernandez FR. 2016. Gain modulation of cholinergic neurons in the medial septum-diagonal band of Broca through hyperpolarization. Hippocampus 1541:1525–1541.

Morris RG, Garrud P, Rawlins JN, O'Keefe J. 1982. Place navigation impaired in rats with hippocampal lesions. Nature 297:681–683.

Nádasdy Z, Hirase H, Czurkó A, Csicsvari J, Buzsáki G. 1999. Replay and time compression of recurring spike sequences in the hippocampus. J Neurosci 19:9497–507.

O'Keefe J. 1976. Place units in the hippocampus of the freely moving rat. Exp Neurol 51:78–109.

O'Keefe J, Burgess N, Donnett JG, Jeffery KJ, Maguire EA. 1998. Place cells, navigational accuracy, and the human hippocampus. Philos Trans R Soc Lond B Biol Sci 353:1333–40.

O'Keefe J, Nadel L. 1978. The Hippocampus as a Cognitive Map. Oxford University Press.

O'Keefe J, Recce ML. 1993. Phase relationship between hippocampal place units and the EEG theta rhythm. Hippocampus 3:317–330.

Patel AX, Burdakov D. 2015. Mechanisms of gain control by voltage-gated channels in intrinsically-firing neurons. PLOS ONE 10:e0115431.

Ranck JB. 1973. Studies on single neurons in dorsal hippocampal formation and septum in unrestrained rats. Exp Neurol 41:532–555.

Ray S, Maunsell JHR. 2011. Different origins of gamma rhythm and high-gamma activity in macaque visual cortex. PLOS Biol 9.

Ridley RM, Barefoot HC, Maclean CJ, Pugh P, Baker HF. 1999. Different effects on learning ability after injection of the cholinergic immunotoxin ME20.4IgG-saporin into the diagonal band of Broca, basal nucleus of Meynert, or both in monkeys. Behav Neurosci 113:303–315.

Scoville WB, Milner B. 1957. Loss of recent memory after bilateral hippocampal lesions. J Neuropsychiatry Clin Neurosci 20:11–21.

Segal M, Barker JL. 1984. Rat hippocampal neurons in culture: Potassium conductances. J Neurophysiol 51:1409–1433.

Simon AP, Poindessous-Jazat F, Dutar P, Epelbaum J, Bassant M-H. 2006. Firing properties of anatomically identified neurons in the medial septum of anesthetized and unanesthetized restrained rats. J Neurosci 26:9038–9046.

Skaggs WE, McNaughton BL, Wilson MA, Barnes CA. 1996. Theta phase precession in hippocampal neuronal populations and the compression of temporal sequences. Hippocampus 6:149–172.

Solstad T, Boccara CN, Kropff E, Moser M-B, Moser EI. 2008. Representation of geometric borders in the entorhinal cortex. Science 322:1865–8.

Sotty F, Danik M, Manseau F, Laplante F, Quirion R, Williams S. 2003. Distinct electrophysiological properties of glutamatergic, cholinergic and GABAergic rat septohippocampal neurons: Novel implications for hippocampal rhythmicity. J Physiol 551.3:927–943.

Squire LR. 1992. Memory and the hippocampus: A synthesis from findings with rats, monkeys, and humans. Psychol Rev 99:195–231.

Stark E, Eichler R, Roux L, Fujisawa S, Rotstein HG, Buzsáki G. 2013. Inhibition-induced theta resonance in cortical circuits. Neuron 80:1263–1276.

Steward O, Scoville SA. 1976. Cells of origin of entorhinal cortical afferents to the hippocampus and fascia dentata of the rat. J Comp Neurol 169:347–370.

Sutherland RJ, McDonald RJ. 1990. Hippocampus, amygdala, and memory deficits in rats. Behav Brain Res 37:57–79.

Sutherland RJ, McDonald RJ, Hill CR, Rudy JW. 1989. Damage to the hippocampal formation in rats selectively impairs the ability to learn cue relationships. Behav Neural Biol 52:331–56.

Tai C, Kuzmiski JB, MacVicar BA. 2006. Muscarinic enhancement of R-type calcium currents in hippocampal CA1 pyramidal neurons. J Neurosci 26:6249–58.

Takács VT, Freund TF, Gulyás AI. 2008. Types and synaptic connections of hippocampal inhibitory neurons reciprocally connected with the medial septum. Eur J Neurosci 28:148–164.

Taube JS. 2007. The head direction signal: Origins and sensory-motor integration. Annu Rev Neurosci 30:181–207.

Taube JS, Muller RU, Ranck JB. 1990. Head-direction cells recorded from the postsubiculum in freely moving rats. I. Description and quantitative analysis. J Neurosci 10:420–35.

Taxidis J, Coombes S, Mason R, Owen MR. 2012. Modeling sharp wave-ripple complexes through a CA3-CA1 network model with chemical synapses. Hippocampus 22:995–1017.

Teles-Grilo Ruivo LM, Mellor JR. 2013. Cholinergic modulation of hippocampal network function. Front Synaptic Neurosci 5:1–15.

Thomson AM, Radpour S. 1991. Excitatory connections between CA1 pyramidal cells revealed by spike triggered averaging in slices of rat hippocampus are partially NMDA receptor mediated. Eur J Neurosci 3:587–601.

Tóth K, Borhegyi Z, Freund TF. 1993. Postsynaptic targets of GABAergic hippocampal neurons in the medial septum-diagonal band of Broca complex. J Neurosci 13:3712–3724.

Tóth K, Freund TF, Miles R. 1997. Disinhibition of rat hippocampal pyramidal cells by GABAergic afferents from the septum. J Physiol 500.2:463–474.

Traub R., Schmitz D, Jefferys JG., Draguhn A. 1999. High-frequency population oscillations are predicted to occur in hippocampal pyramidal neuronal networks interconnected by axoaxonal gap junctions. Neuroscience 92:407–426.

Traub RD, Bibbig A. 2000. A model of high-frequency ripples in the hippocampus based on synaptic coupling plus axon-axon gap junctions between pyramidal neurons. J Neurosci 20:2086–2093.

Vandecasteele M, Varga V, Berényi A, Papp E, Barthó P, Venance L, Freund TF, Buzsáki G. 2014. Optogenetic activation of septal cholinergic neurons suppresses sharp wave ripples and enhances theta oscillations in the hippocampus. Proc Natl Acad Sci U S A 111:13535–13540.

Wei Y, Krishnan GP, Bazhenov M. 2016. Synaptic mechanisms of memory consolidation during sleep slow oscillations. J Neurosci 36:4231–4247.

Wilson MA, McNaughton BL. 1994. Reactivation of hippocampal ensemble memories during sleep. Science 265:676–9.

Winson J. 1978. Loss of hippocampal theta rhythm results in spatial memory deficit in the rat. Science 201:160–163.

Witter MP, Amaral DG. 1991. Entorhinal cortex of the monkey: V. Projections to the dentate gyrus, hippocampus, and subicular complex. J Comp Neurol 307:437–459.

Zhang H, Lin S-C, Nicolelis MAL. 2010. Spatiotemporal coupling between hippocampal acetylcholine release and theta oscillations *in vivo*. J Neurosci 30:13431–40.

Zhang H, Lin S-C, Nicolelis MAL. 2011. A distinctive subpopulation of medial septal slow-firing neurons promote hippocampal activation and theta oscillations. J

Neurophysiol 106:2749–63.

Zhong C, Talmage DA, Role LW. 2013. Nicotine elicits prolonged calcium signaling along ventral hippocampal axons. PLOS ONE 8:1–14.